Processes of lateral moraine formation at a debris-covered glacier, Suldenferner (Vedretta di Solda), Italy

Monika Rabanser

Dissertations in Geology at Lund University,
Master's thesis, no 556
(45 hp/ECTS credits)

Processes of lateral moraine formation at a debris-covered glacier, Suldenferner (Vedretta di Solda), Italy

Master's thesis
Monika Rabanser

Department of Geology
Lund University
2019

Contents

Cover Picture: Close-up photograph of the western lateral moraine at Suldenferner (Vedretta di Solda), Italy.
Photo: Monika Rabanser.

Processes of lateral moraine formation at a debris-covered glacier, Suldenferner (Vedretta di Solda), Italy

MONIKA RABANSER

Abstract: Lateral moraines are key features of glacial landscapes in high-alpine mountain areas. Research on lateral moraine formation is mostly limited to clean-ice glaciers; lateral moraine formation at the margins of debris-covered glaciers is currently poorly understood in an Alpine and sedimentological context. This thesis focuses on the reconstruction of processes of lateral moraine formation at the debris-covered glacier Suldenferner (Vedretta di Solda) in NE Italy. The most important geomorphological elements of the Suldenferner foreland are: (i) the lateral moraines, (ii) former areas of stagnant ice, (iii) a moraine from 1927, (iv) ice-moulded bedrock giving the direction of ice-flow, (v) outwash terraces, (vi) erosional remnants of the lateral moraines, (vii) gullied glaciogenic material and (vii) glacially-overridden outwash.

The studied lateral moraines at Suldenferner reach heights between 110 and 130 m above their bases and are up to 3 km wide. The eastern lateral moraine is characterised by a pronounced cross-profile asymmetry, with gentle distal slopes (14°-30°) and steeper proximal slopes (40°-60°), while the western lateral moraine is only slightly asymmetrical, with steep slopes ranging between 60°-80°. Clasts within the lateral moraine along the western margin of the glacier are exclusively dolomite, while the clasts within the lateral moraine along the eastern margin of the glacier contain mainly micaschist, with some dolomite and paragneiss.

Sediments within the lateral moraines are divided into three lithofacies associations: *lithofacies association 1 (LFA 1)* is a silty-sandy, matrix-supported diamicton (DgMm$_3$-2), *lithofacies association 2 (LFA 2)* comprises a clayey-silty, massive diamicton (DgFm$_2$-2) and a clayey-silty, matrix-supported diamicton (DhMm$_3$-2) and *lithofacies association 3 (LFA 3)* is a sandy-gravelly, clast-rich diamicton (DmCm$_1$-1, DmCm$_2$-1). These lithofacies associations are interpreted as reworked, glaciofluvial deposits (*LFA 1*), subaerial debris flows that have been stacked in an ice-marginal position (*LFA 2*) and debris flows that have incorporated distinctive amounts of micaschist (*LFA 3*).

Clast shape analysis reveals that the sediment delivery towards the lateral moraines contains a signal of mixed sources: the main mode of transport consists of subglacial and englacial sources (active transport), aided by minor contributions of supraglacial/extraglacial sources (passive transport). The presented conceptional model for lateral moraine formation in the Alps highlights the value of active clast delivery, whiles the importance of a supraglacial debris cover, and its final emplacement into laterally forming moraine ridges, exerts a limited influence on the moraine's sedimentology. The model implies that lateral moraines have a complex formation history with glacier fluctuations, characterised by multiple glacial advance and retreat cycles.

.

Monika Rabanser, Department of Geology, Lund University, Sölvegatan 12, SE-223 62 Lund, Sweden. E-mail: monika.rabanser@yahoo.com

Lateralmoräners bildningsprocesser vid en sedimenttäckt glaciär, Suldenferner (Vedretta di Solda), Italien

MONIKA RABANSER

Sammanfattning: Lateralmoräner är karaktäristiska för glaciala landskap bildade i höga bergsområden med dalglaciärer. Forskningen om lateralmoräners bildning är dock ofta begränsatsade till glaciärisar med lågt materialinnehåll. När lateralmoräner bildas längs kanten av materialrika glaciärer, med det glaciala materialet i sin senare fas huvudsakligen transporterat över glaciärens yta tillkommer sedimentationsprocesser som delvis är dåligt utforskade. Föreliggande arbete fokuserar på rekonstruktionen av de processer som är aktiva för bildandet av lateralmoräner vid den sedimenttäckta glaciären Suldenferner (Vedretta di Solda) i nordöstra Italien. De viktigaste geomorfologiska elementen i förlandet av Suldenferner-glaciären är (i) lateralamoräner, (ii) ett område med stagnant is, (iii) en moränrygg bildad 1927, (iv) isskulpterad berggrund med isflödesriktningsindikationer, (v) glacifluviala smältvattenterrasser, (vi) erosionsrester av lateralmoräner, (vii) smältvattenkanaler i glacigent material och (vii) glaciäröverskrida smältvattensediment.

De lateralmoräner som har studerats vid Suldenferner-glaciären reser sig mellan 110 och 130 från sin bas och är upp till 3 km breda. De kännetecknas av en uttalad tvärprofilsasymmetri med en svagt lutande distalsluttning (14˚-30˚) och en mer brant lutande proximalsluttning (40˚-80˚). Sten och block i lateralmoränen längs kanten av glaciären består uteslutande av dolomit, medan klastermaterialet i lateralmoränen längs den östra glaciärkanten huvudsakligen består av glimmerskiffer, dolomit och paragnejs.

Sedimenten som bygger upp lateralmoränerna har delats in i the sedimentfacie: *litofacies association 1 (LFA 1)* består av en siltig-sandig, matrix-stödd diamikt (DgMm$_3$-2), *litofacies association 2 (LFA 2)* innehålle en lerig-siltig, massiv diamikt (DgFm$_2$-2) och en lerig-siltig, matrix-stödd diamikt (DhMm$_3$-2) och *litofacies association 3 (LFA 3)* är sandig-grusig, klaster-rik diamikt (DmCm$_1$-1 och DmCm$_2$-2). Dessa sedimentfacies tolkas processgenetiskt som glacialt omarbetade, glacifluviala sediment (*LFA 1*), subaerila flytjordssediment, vertikalt ackumulerade i ismarginalt läge (*LFA 2*) och, slutligen, flytjordssediment med stort tillskott av jordströmmar med inslag av stenfalls-processer (*LFA 3*).

Formanalys av claster visar att sedimentleveransen mot laterala moränerna skett från blandade källor. Det huvudsakliga transportsättet består av subglacial och englacial aktiv transport av klastermaterial med mindre bidrag från supraglaciala källor (passiv transport). Den presenterade konceptuella modellen för lateral-moränbildning i Alperna belyser betydelsen av aktiv klastertillförsel, medan vikten av supraglacial klastertillförsel och dessas slutliga avsättning i de lateralt bildande moränsryggarna utövar ett begränsat inflytande på moränsryggarnas sedimentologi. Den presenterade konceptuella modellen påvisar att lateralmoränerna vid Suldenferner-glaciären har en komplex bildhistoria med glaciärfluktuationer-kännetecknade av flera glaciala framstöts-och reträttcykler.

Monika Rabanser, Geologiska institutionen, Lunds universitet, Sölvegatan 12, SE-223 62 Lund, Sverige. E-post: monika.rabanser@yahoo.com

1 Introduction

Lateral moraines are outstanding features in glacial landscapes throughout the world (Small, 1983; McMahon, 2015; Tonkin, 2016). Because lateral moraines mark ice-marginal fluctuations (advance and retreat cycles) they allow the reconstruction of the glacial history in high-mountain areas. Lateral moraine formation can be regarded as a complex and time-transgressive process, frequently occurring over centennial timescales (Benn et al., 2003). Even if the crucial role of lateral moraines for modelling glacial dynamics is undisputed, there is a substantial lack in sedimentological studies of lateral moraine formation in high-alpine settings (see Lukas et al., 2012 for a review). In fact, the understanding of the genetic processes that significantly modulate the development of these glacial landforms is poor (Benn and Owen, 2000; Evans et al., 2010).

Lateral moraines are regarded as key features within the "glaciated valley landsystem" (Boulton and Eyles, 1979). Moraine genesis within this landsystem was initially attributed to release of debris that had been transported predominantly supraglacially (passively) (Benn et al., 2003; Hambrey et al., 2009; Benn and Evans, 2010). These concepts have been adopted uncritically for at least a decade (Vere and Benn, 1989; Benn and Ballantyne, 1994). However, detailed studies in Iceland (e.g. at Kvíárjökull, Spedding and Evans, 2002) and Switzerland (e.g. at Findelengletscher, Lukas et al., 2012) have shown that the processes and transport pathways are more complex than previously predicted. Most of the recent studies in high-mountain environments, like the European Alps (e.g. Lukas and Sass, 2011; Lukas et al., 2012; McMahon, 2015, 2016) have focused on clean-ice glaciers, which are the types normally found in the Alps. These studies specifically highlight the importance of a subglacial (active) debris transport at clean-ice glaciers. However, little is known about the behaviour of debris-covered glaciers, despite multiple studies in the Himalayas (Shroder et al., 2000; Scherler et al., 2011; Benn et al., 2012) and in the Mont Blanc Massif (Brock et al., 2010). Debris-covered glaciers react remarkably differently to climate fluctuations compared to clean-ice glaciers due to reduced ablation rates—essentially debris cover modulates the climatic signal non-linearly (Benn and Evans, 2010; Kellerer-Pirkelbauer et al., 2008; Brook and Lukas, 2012). Thus, the link between the geological evidence (lateral moraines) and reconstructing the history of glacier fluctuations from this evidence is more complicated than in clean-ice glaciers. Therefore, a modern re-evaluation of the sediment transport pathways at debris-covered glaciers is required to explain the genesis of lateral moraines in high-alpine settings. This thesis focuses on a study area located in the Ortler-Alps, more precisely in the foreland of the debris-covered glacier Suldenferner (Vedretta di Solda) in northern Italy. The aim of this thesis is threefold. The first goal is to record the geomorphological and geological signature of a high-alpine, debris-covered glacier in the Eastern European Alps. The second aim is to understand the genesis of large lateral moraines at debris-covered glaciers. The third goal is to reconstruct the sediment pathways that favour the debris delivery towards the moraines.

2 The Dynamics of Debris-covered Glaciers: Implications for Suldenferner's Development

It has been shown that the thickness of a supraglacial debris cover plays a crucial role in influencing a glacier's mass balance while causing differential surface melt (Popovnin and Rozova, 2002). Debris covers of > 5 cm in thickness insulate the glacier from incoming insolation, whereas a sparse debris cover (< 5 cm) favours glacial melt via a significant decline in albedo and an increased absorption of shortwave radiation (Nakawo and Young, 1981; Kirkbride and Dugmore, 2003). Indeed, debris-covered glaciers generally have a remarkably lower albedo (around 0.1) than clean-ice glaciers (between 0.35-0.55, Patterson and Cuffey, 2010). This results in an altered energy balance of debris-covered glaciers, where moisture exchange and sensible heat flux occur exclusively (Haidong et al., 2006). Variations in debris thickness are reflected in increased debris layer volumes in down-glacier areas. This is due to a higher accumulation of melt-out debris and a progressive decrease in ice-flow velocity (Collier et al., 2015) and results in a reversion of the ablation gradient (small ablation rates at the glacier terminus, Benn et al., 2003). In fact, the terminus position of debris-covered glaciers is designated to be stable for longer periods than observed at clean-ice glaciers (Patterson and Cuffey, 2010). Because the porosity of debris layers decreases with increasing depths—accompanied by a rising water content—temperature gradients diminish with increasing debris thickness (Nagai et al., 2013). While clean-ice glaciers are characterised by a nearly linear mass balance variation plotted against elevation (due to the linear behaviour of temperature dependent melting), debris-covered glaciers behave in an exponential mode (Scherler et al., 2011). The differential melting of debris-covered glaciers is the main reason for an uneven surface on top of these glaciers (Reynolds, 2000). Glaciers that are covered with extensive debris covers are frequently
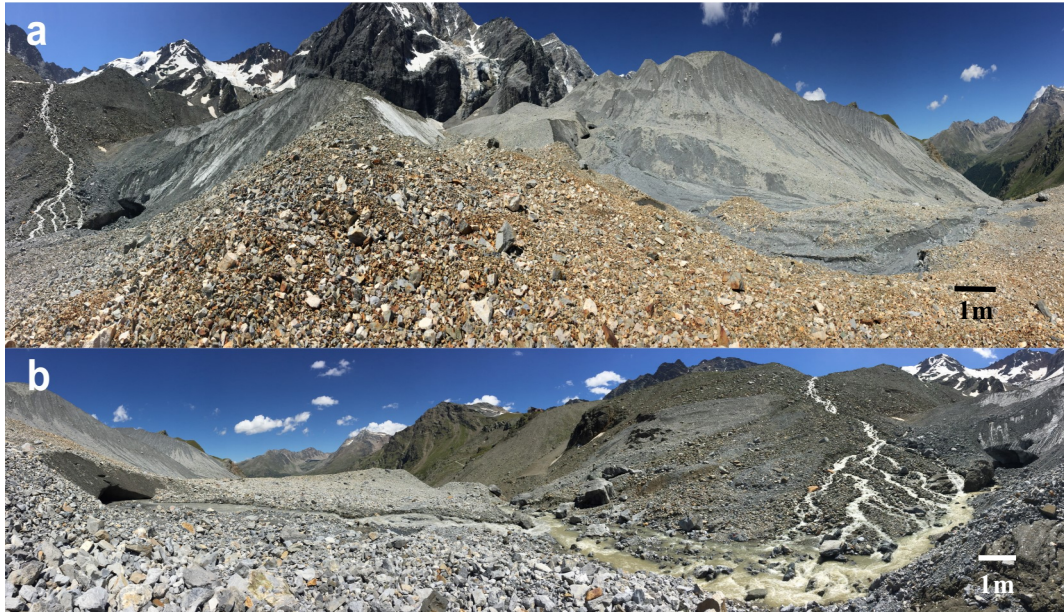
Fig. 1. Ice-marginal area of Suldenferner. (a) Supraglacial debris cover, view towards SW. (b) Glacier portal and meltwater streams, migrating valley-downwards, view towards NW.

characterised by a steady front and a stagnant tongue. Contrarily, clean-ice glaciers do not show this type of behaviour (Scherler et al., 2011). Moreover, debris-covered glaciers are characterised by a longer and thinner ablation zone as compared to clean-ice glaciers (Haidong, 2006; Scherler et al., 2011). At Suldenferner more than 50% of the total debris cover reaches thicknesses between 6 and 16 cm (L.I. Nicholson, pers. comm., 2018). Due to these debris properties the impact of atmospheric heat is vitally reduced, contributing to an enhanced preservation potential of the glacier under the present boundary conditions. This is in contrast to many clean-ice glaciers in high-alpine settings (e.g. Lukas et al., 2012). The close surroundings of Suldenferner are characterised by abundant areas of discontinuous permafrost that are susceptible to global climate change (Stötter et al. 2003). Personal field observations from 2018 suggest that the main source of debris delivery at Suldenferner is retrieved from rockfall, avalanches and steep icefalls above a gently sloping ablation zone (Fig. 1a). Steep, overhanging rock walls are abundant in both the southwest and east of the study area, that provide the top of the glacier with a continuous amount of debris. Here, the dolomite walls in the southwest are the main debris delivery source for Suldenferner, even though some micaschist and paragneiss (in the east of the study area) are delivered towards the glacier snout in the form of supraglacial debris. This field evidence is specifically visible in a remarkable colour contrast between grey dolomite pebbles and brown micaschist/paragneiss sources (Fig. 1a, 1b). Diurnal freeze-thaw cycles and temperature fluctuations which favour frost shattering (Nagai et al., 2013) further ensure a constant debris delivery towards Suldenferner's terminus.

3 Study Area

The area of interest is set in the foreland of Suldenferner (Vedretta di Solda), a debris-covered glacier in the Ortler-Cevedale group (Eastern European Alps, northern Italy, Fig. 2). Suldenferner (46° 29`24``N 10° 33`36``E) extends over altitudes between 3,900 m and 2,410 m and belongs to the Stilfserjoch National Park in the Autonomous Province of South Tyrol (northern Italy, Fig. 3c).

Data about the glacier have been retrieved regularly throughout the last decades (Nicolussi and Stötter, 1995; Stötter et al., 2003; Knoll and Kerschner, 2009). Recent investigations by Nicholson (2015) resulted in accurate quantifications of the glacier extent (most areas showing a surface change between 0 and +5m) and its supraglacial debris thickness (total range: 3-67 cm). Moreover, the Bottom Temperature of Snow Cover (BTS, around -0.5°C) has been measured in order to predict the Winter Equilibrium Temperature (WEqT, between -0.2 and -2.8°C) at Suldenferners' snout (Nicholson, 2015).

South Tyrol is characterised by unique tectonic and stratigraphic features. (Fig. 3). The south of the region is dominated by magmatic and sedimentary bedrock (South-Alpine unit), whereas the north almost exclusively contains outcrops of metamorphic bedrock (former European continent, East-Alpine unit). These units are separated by one of the most prominent tectonic structure in the Alps, the "Periadriatic suture" (Mair and Stingl, 2014). The collision between the Adriatic plate with the European continent caused a thrusting of the East-Alpine unit upon the Penninic nappes. This event took place during the main Alpine orogeny at 160 Ma.
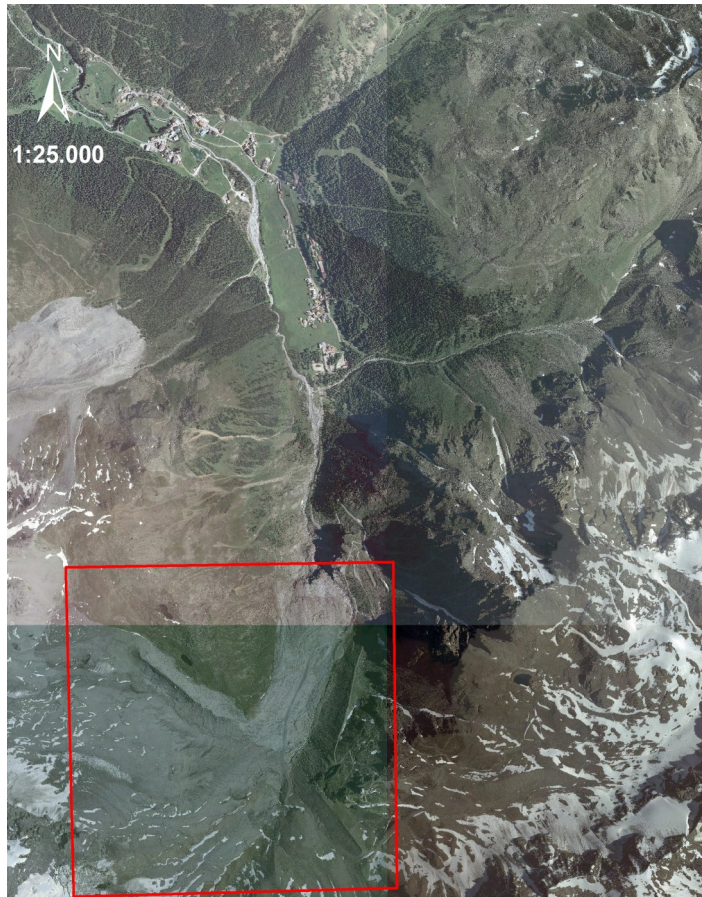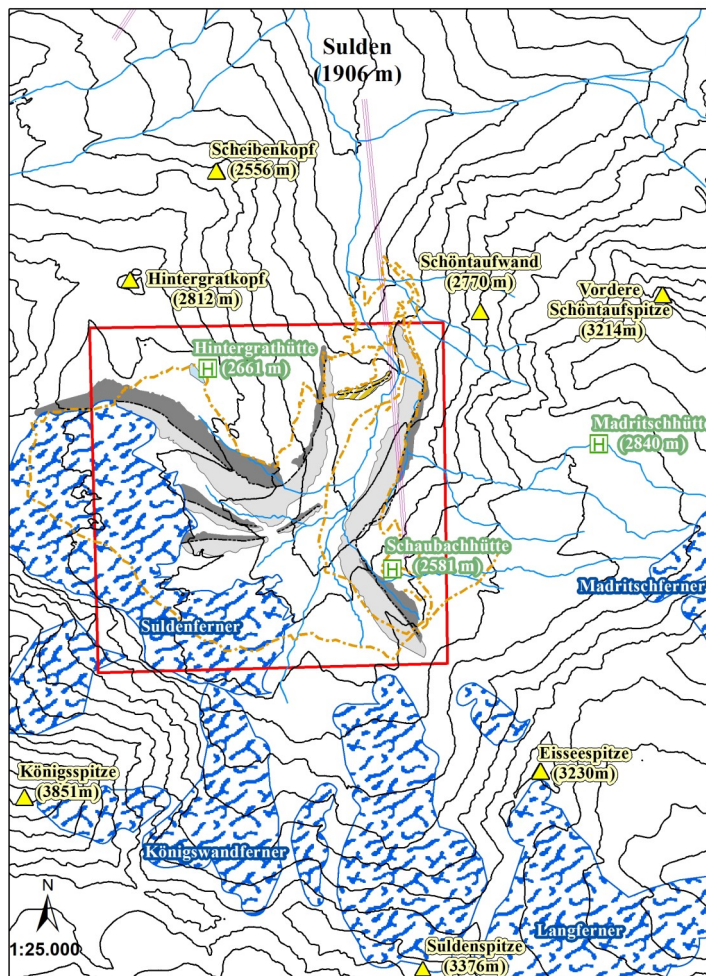
Fig. 2. Context maps depicting the surroundings of Suldenferner, NE Italy. The study area is marked by a red rectangle. (a) Orthofoto of 2011, Scale 1:25,000. (b) Map supplemented with contour lines, prominent peaks and major glacial bodies.

Fig. 3. Study area. (a) Large-scale European basemap.(b) National context map of northern Italy, supplemented with major central-European states. (c) Regional context map of South Tyrol.

Legend

Quaternary continental deposits
Alpine Molasse
Tertiary plutons

PENNINIC UNITS

Helvetic units
Arosa-Zone (Flysch Cretaceus-Eocene)
Tasna nappe (Trias-Eocene with basement)
Calcschists with ophiolitic bodies
Old European basement nappes
Central Gneiss

SOUTHERN ALPS

Cretaceous-paleogene sediments
Permo-jurassic sediments
Triassic vulcanites and volcanoclastites
Triassic plutons
Permian vulcanites
Permian plutons
Paleozoic succesion (Alpi Carniche)

Periadriatic Line
Tectonic lines
Thrusts of mayor units
Minor thrusts
Thrusts with reactivation as normal fault
Normal faults
Strike-slip faults

Low grade metamorphic Variscan basement
Medium grade metamorphic Variscan basement

AUSTROALPINE UNITS

Permo-mesozoic succession of the Northern Calcareous Alps
Northern paleozoic succession (Grauwackenzone)
Permo-mesozoic succession of different tectonic units
Permian plutons

CRYSTALLINE BASEMENT

Steinach nappe (St) (Low variscan and alpine metamorphic grade)
Thurntaler unit (Th) (Medium variscan and negligible alpine metamorphic grade)
Antholz unit (A) (Medium-high variscan and negligible alpine metamorphic grade)
Tectonic units of Passaier (P) (Medium-high variscan and negligible alpine metamorphic grade)

Marlinger unit (M) (Medium-high variscan and low alpine metamorphic grade)
Tonale nappe (T) (High variscan and negligible alpine metamorphic grade)
Ötztal nappe (Ö) (Medium-high variscan and medium-low alpine metamorphic grade)
Schneeberg unit (S) (Medium-high alpine metamorphic grade)
Texel unit (Tx) (High variscan and alpine metamorphic grade)

Taufers unit (Tu) (Medium-high variscan and alpine metamorphic grade)
Zebrù unit (Z) (Low variscan and negligible alpine metamorphic grade)
Ortles-Campo nappe (C) (Medium-high variscan and low alpine metamorphic grade)
Taufers unit (Tu) (Medium-high variscan and alpine metamorphic grade)
Zebrù unit (Z) (Low variscan and negligible alpine metamorphic grade)
Ortles-Campo nappe (C) (Medium-high variscan and low alpine metamorphic grade)
Vinschgau shear zone
Sesvenna unit (Sv) (Medium-high variscan and negligible alpine metamorphic grade)
Silvretta nappe (Si) (Medium-high variscan and medium alpine metamorphic grade)
Innsbruck (I) and Landeck (L) phyllite (Low variscan and negligible alpine metamorphic grade)
Bernina nappe (B) (Medium-high variscan and low alpine metamorphic grade)

Fig. 4. Bedrock geology of South Tyrol and its surroundings. Modified after Keim, Mair and Morelli (2017).

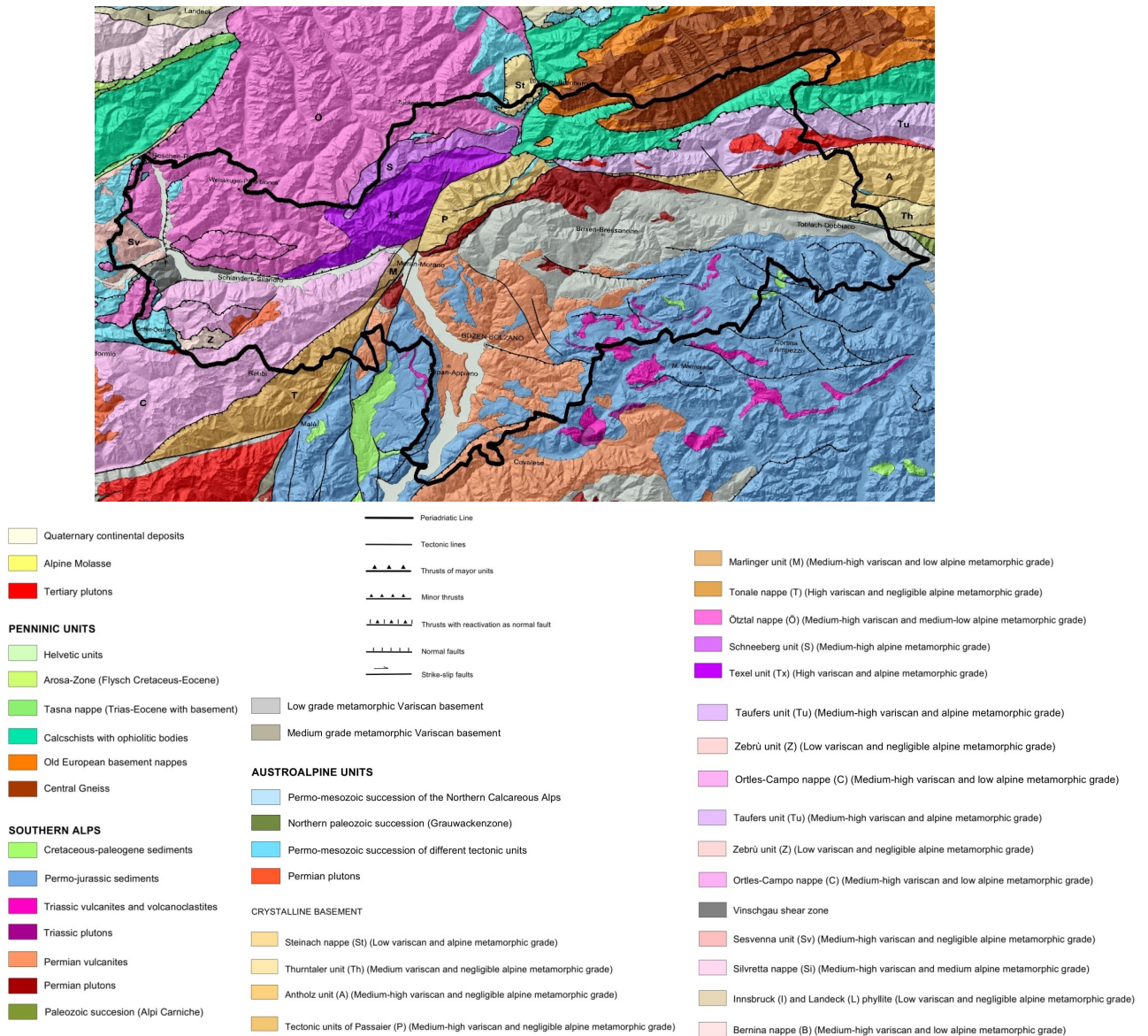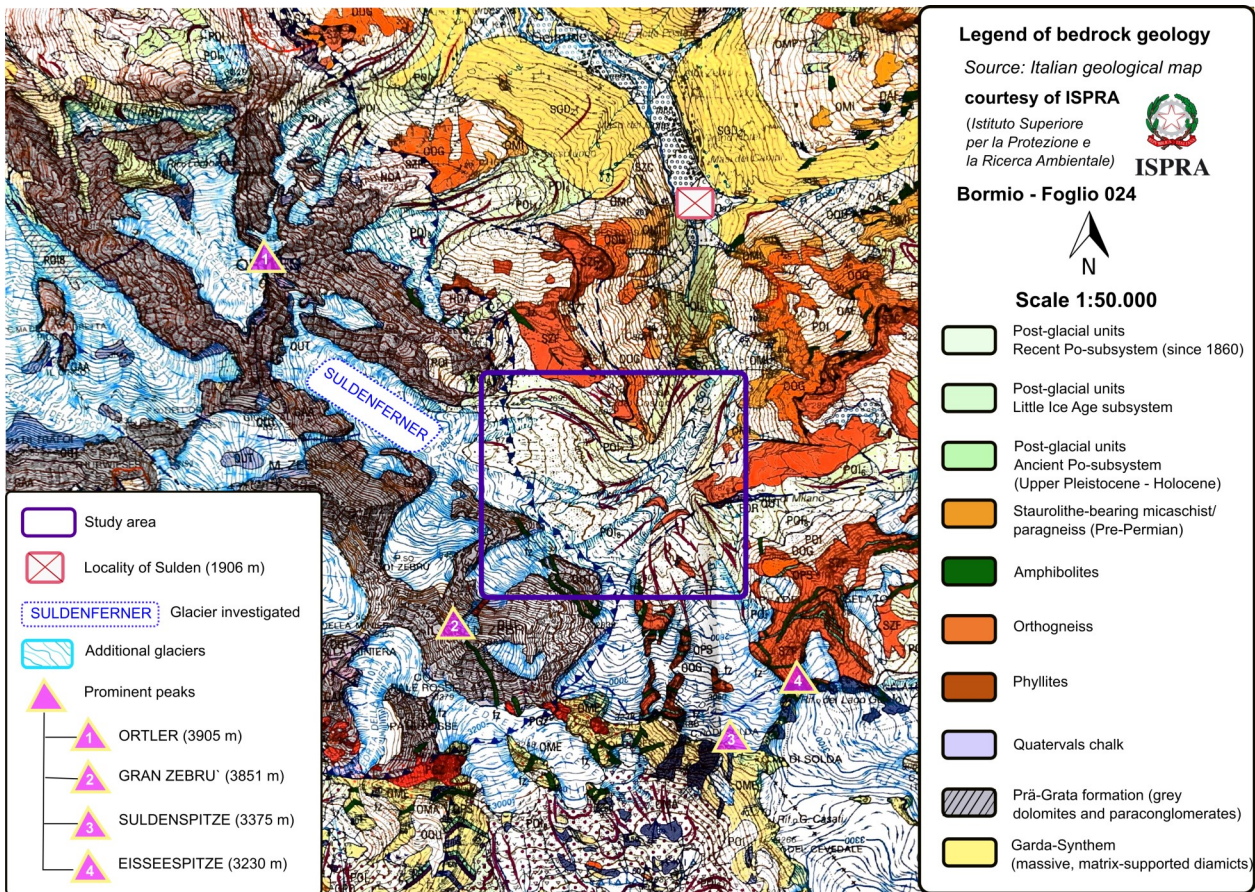*Fig. 5.* Bedrock geology of the study area (Courtesy of ISPRA. Modified after Montrasio et al., 2012).

The East-Alpine represents the northern-rim of the Adriatic microcontinent (Apulian plate). Remnants of a former sedimentary Mesozoic drape are preserved as the Ortler-Cevedale group. At around 30 Ma, tonalitic intrusions altered the structure of these units. Sedimentary rocks (mainly limestone and dolomite) prevail in the northwestern area of the Ortler-Cevedale group and form sharp aretes. In contrast, the eastern parts are characterized by the appearance of metamorphic rocks (paragneiss, micaschist, phyllites), forming rounded features (Montrasio et al., 2012; Fig. 5).

The contrasting nature in lithology has significant effect on both terrain morphology and the general distribution of the present glaciers in the Ortler-Cevedale group (Desio, 1967). Today, Suldenferner covers a total area of 6.5 km² and it is considered the biggest glacier in the Upper Sulden Valley (Stötter et al., 2003). The adjacent glaciers (Königswandferner and Madritschferner) occupy less than 1 km² of area (Carturan et al., 2013). Suldenferner consists of three branches: the western Ortler stream, the middle Königsspitze stream and the eastern Königsspitze stream (Fig. 5). The glaciers of the Ortler-Cevedale group are particularly important for the local population due to their touristic appeal and their status as precious water resources (Carturan et al., 2013). Nowadays Suldenferner's foreland is artificially altered by ski slopes and walking paths (Fig. 6) and it is accessible via a cable car that runs from the locality of Sulden (valley station, 1906 m) up to the Schaubach hut (mountain station, 2581 m). As being one of the biggest glacierized

areas of the Southern European Alps (76.8 km²) the glaciers in the Upper Sulden valley have been continuously retreating since the Little Ice Age and specifically Suldenferner is characterised by multiple advance and retreat cycles (Table 1, Fig. 7, Stötter et al., 2003; Citterio et al., 2007).

Table 1. Summary of Suldenferners glacial fluctuations between 1819 and today. Reconstructed development of absolute area (km²) and relative area (%). Modified after Stötter et al. (2003).

Time period	Glacial behaviour	Absolute area (km²)	Relative area (%)
Until 1819	Advance	9.56	100
1819-1846	Retreat		
1846-1858	Advance	9.83	92.4
1858-1890	Retreat		
1890-1903	Advance	8.11	84.8
1903-1915	Retreat		
1915-1927	Advance	8.12	84.9
1927-1972	Retreat		
1972-1975	Stationary		
1975-1987	Advance	6.47	67.7
Since 1987	Retreat		
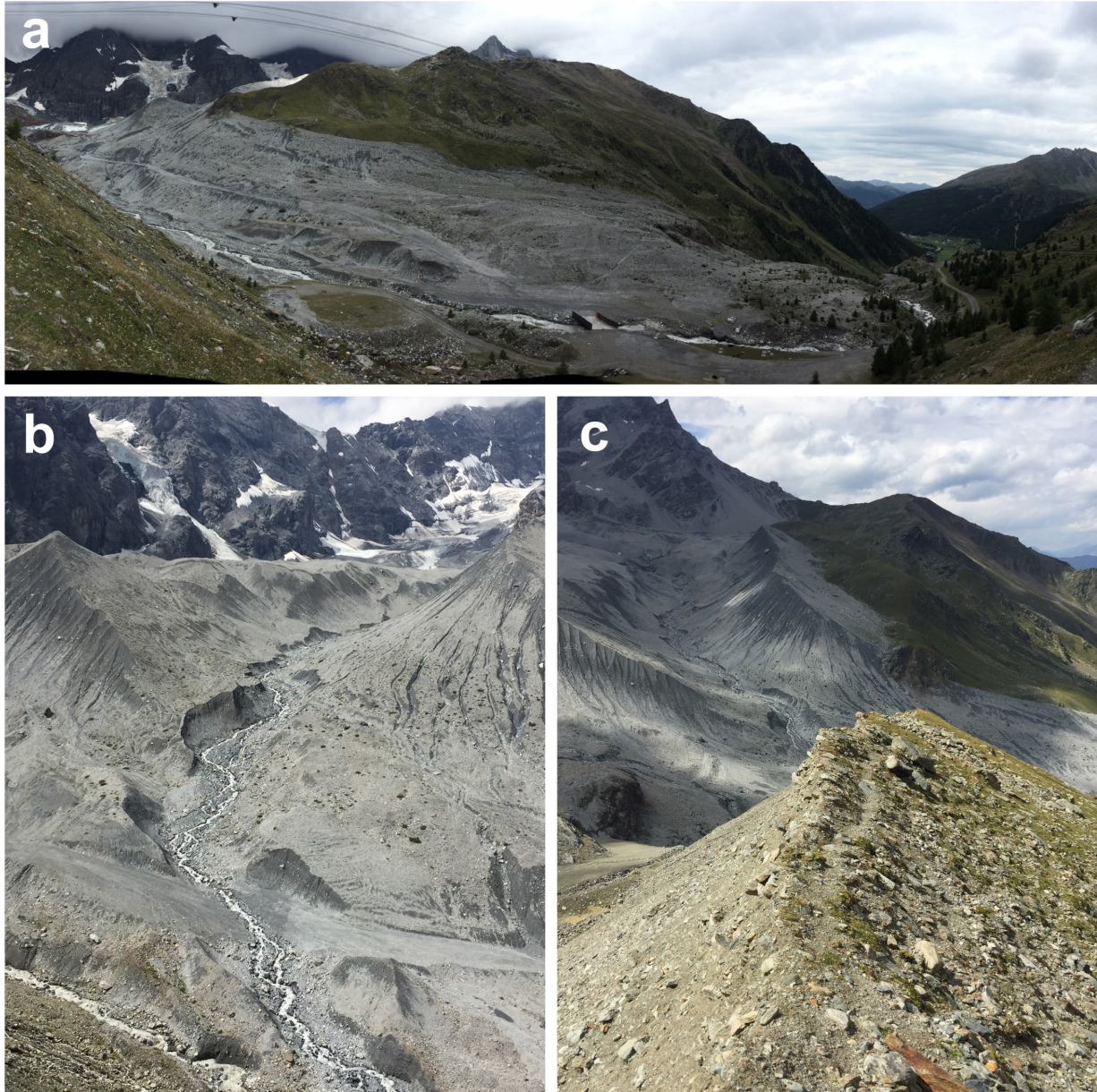
Fig. 6. Close-up photographs of the lateral moraines at Suldenferner. (a) Overview of the Suldenferner foreland (view towards W). (b) Main branch of the western lateral moraine separated by a series of subsidiary ridges (view towards SW). (c) Northern rim of the eastern lateral moraine (view towards W).

Radiocarbon dating of a buried larch stem revealed that a Medieval glacier advance of Suldenferner occurred at around 800 AD (Nicolussi and Stötter, 1995). Subsequently, stages of temporary re-advances of the glacier occurred during the 1890s, 1910-1920s and in the 1970s-1980s (Carturan et al., 2013). The glacier advance until 1819 was characterised by a maximum surge with velocities of 2 m/day until the valley station of the modern cable car (Fig. 8). In contrast, the advance between 1846 and 1858 ended approximately 500-600 m behind the maximum extent of the 1819 advance. The glacial retreat after 1920 resulted in the formation of a moraine ridge (1927) that is clearly identifiable in the field and in aerial photographs (cf.

Fig. 2a). In general, the Suldenferner foreland is characterised by multiple accumulations of openwork gravel represents a challenge in safely obtaining sedimentological samples (Fig. 9). The current phase of Suldenferner's intense retreat initiated in the second half of the 1980s (Citterio et al., 2007). It is interesting to note that differences in ice volume are remarkably lower in 19th century as compared to the 20th century. The average loss in ice thickness between 1820 and 1985 accounts approximately 29 m of ice (Stötter et al., 2003; Table 1, Fig. 10). Approximately 2/3 (equivalent to 18 m) of ice volume has vanished between 1906 and 1985. Further, the average loss in ice thickness between 1820 and 1906 is estimated to be

Fig. 7. Comparison between historical archives and modern images of Suldenferner. (a) View towards the Königsspitze (Gran Zebrù) from the Düsseldorfer hut (comparison between 1900 and 2015). (b) Panorama image of Suldenferner, Schaubach hut visible in the bottom left corner, view towards the Königsspitze (1913 compared to 2015). Archives of the Geological Service of South Tyrol. Courtesy of Volkmar Mair (2018).

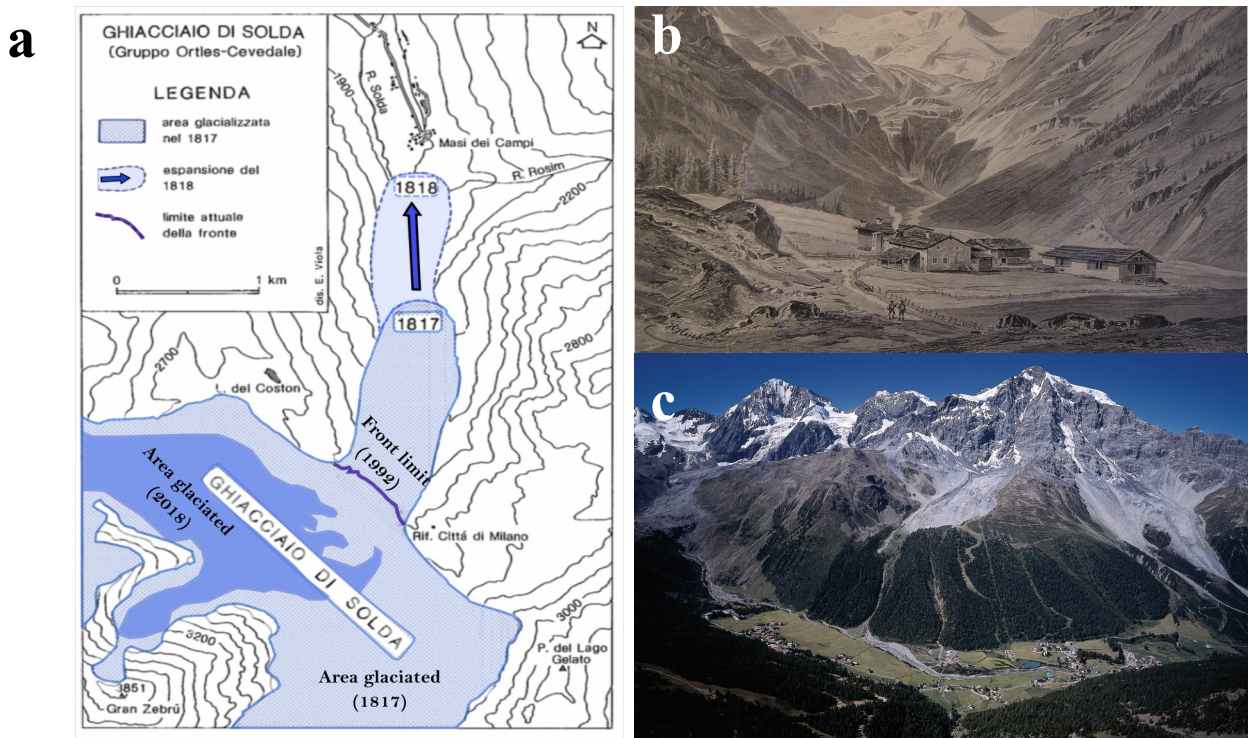*Fig. 8.* (a) Map of Suldenferner, showing the spectacular snout advance between 1817-1818. The glacier increased its length around 1,200 m (modified after Dutto and Montara, 1992). (b) Historical painting of the locality of Sulden (Gampenhöfe) after B. Beubner (1920). (c) Panorama image of the Sulden valley from 2008, view towards the Königsspitze and the Ortler (Geological Service of South Tyrol, 2018).

13

Fig. 9. Close-up images of Suldenferner. (a) Depressions, marking river migration (view towards NE). (b) Stiff diamicton, draped by angular boulders (western lateral moraine, view towards NW). (c) Excavation at the bottom part of the eastern lateral moraine (view towards N). (d) Debris cover on the western edge of Suldenferner glacier (view towards E).

14
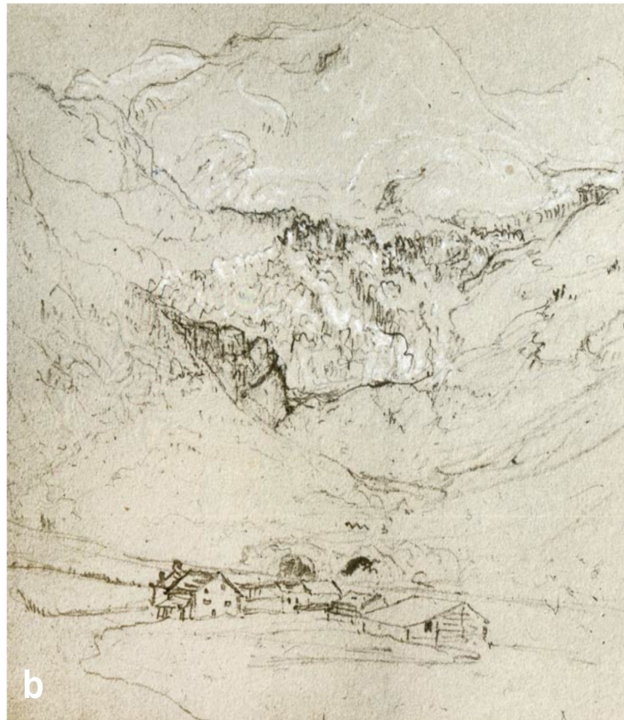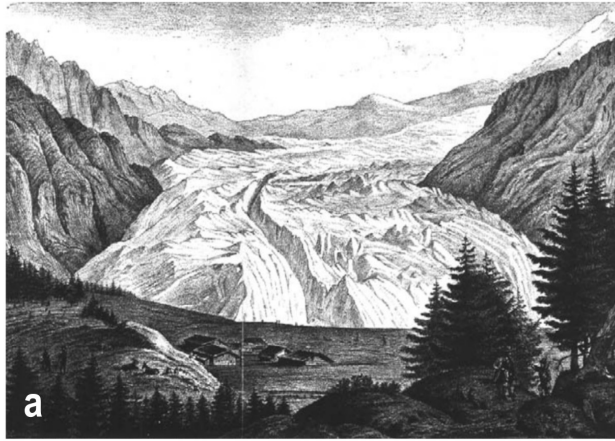
Fig. 10. Historical drawings and photographs of Suldenferner. (a) Glacier snout of advancing Suldenferner of 1818 (drawing of Sebastian Finsterwalder). (b) "Sulden-glacier" painting of Thomas Dyke Acland (1946, Tiroler Landesmuseum Ferdinandeum). (c) Glacier snout of advancing Suldenferner of 1855. Drawing of Friedrich Simony (1881). (d) "Tyrol- The Sulden valley close to St. Gertraud" photograph of Bernhard Johannes (1875/76). (e) End of Sulden valley (unknown author, 1886). (f) Glacier snout of Suldenferner (photograph of Sebastian Finsterwalder, 1906).
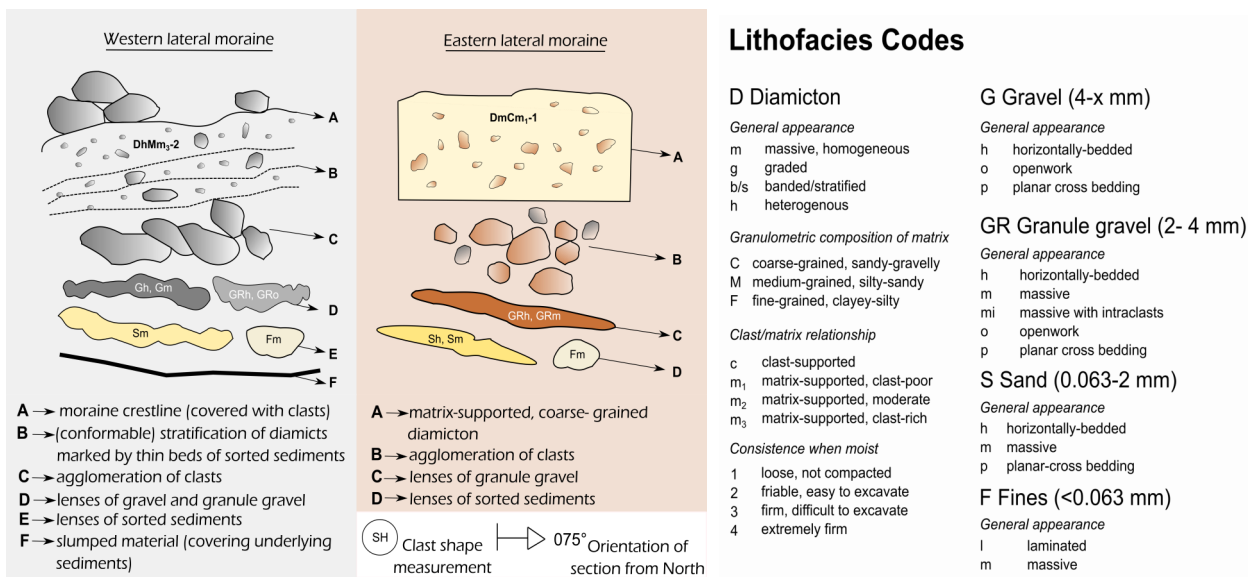
15

Lithofacies Codes

D Diamicton

General appearance

m	massive, homogeneous
g	graded
b/s	banded/stratified
h	heterogenous

Granulometric composition of matrix

C	coarse-grained, sandy-gravelly
M	medium-grained, silty-sandy
F	fine-grained, clayey-silty

Clast/matrix relationship

c	clast-supported
m_1	matrix-supported, clast-poor
m_2	matrix-supported, moderate
m_3	matrix-supported, clast-rich

Consistence when moist

1	loose, not compacted
2	friable, easy to excavate
3	firm, difficult to excavate
4	extremely firm

G Gravel (4-x mm)

General appearance

h	horizontally-bedded
o	openwork
p	planar cross bedding

GR Granule gravel (2- 4 mm)

General appearance

h	horizontally-bedded
m	massive
mi	massive with intraclasts
o	openwork
p	planar cross bedding

S Sand (0.063-2 mm)

General appearance

h	horizontally-bedded
m	massive
p	planar-cross bedding

F Fines (<0.063 mm)

General appearance

l	laminated
m	massive

Fig. 11. Key to sedimentological logs used in this study. Modified from Krüger and Kjaer (1999).

13.3 m of ice. It turns out that the yearly average loss in ice thickness is quite high in the ablation zone (1m) and lower in the accumulation zone (20 cm) of the glacier (Stötter et al., 2003).

4 Methods

In order to achieve the aims of this master thesis a broad range of geomorphological and sedimentological methods were used. These include the following approaches that are described in detail below.

4.1 Geomorphological Mapping

The mapping procedure of the glacial foreland was conducted at a scale of 1:12,000 (from enlarged topographical basemaps at a scale of 1:25,000). Mapping was conducted according to approaches suggested by Chandler et al. (2018). The geological and geomorphological maps were further supplemented with orthophotos (LiDAR images with a horizontal ground resolution of 2.5 m) and hillshades (2.5 m horizontal ground resolution) that have been retrieved by the Geological Service of South Tyrol (2018). The orthophotos originate from flight campaigns during both summer (2003, 2008, 2011) and winter (2000-2001, 2014-2015) seasons.

To gain further knowledge about ice-marginal fluctuations historical archives were considered (Nicolussi and Stötter, 1995; Stötter et al. 2003) and ice-marginal fluctuations of the past 30 years (i.e. 1988-2018) were assessed. Field mapping was progressively digitised using the ArcGIS 10.0 software to ensure planimetric accuracy. The knowledge gained from cartographic analysis was subsequently used to explain the formation of the lateral moraines at Suldenferner and the debris delivery from the glacier

portal to the snout. Glaciological evidence, comprising Suldenferner's development between 2014 and 2018 (L.I. Nicholson, pers. comm., 2018) was further applied to shed light on the present stability of the debris-covered glacier.

4.2 Sedimentology: Logging

The exposures in the moraines were created in a similar way as the sedimentological investigations at Findelengletscher (see Lukas et al., 2012 for a review). Single sections were dug by hand with a spade and a trenching tool. The presence of large gullies within the western lateral moraine facilitated the digging process by providing shallow slumps above natural exposures. Initially, surface cleaning was conducted while scraping unconsolidated superficial material to get to the in-situ sediment. Drawings of the exposures were established on millimeter paper, using a tape measure hung from the top of the section to establish a vertical scale (Evans and Benn, 2004; Lukas et al., 2012). The most prominent boulders and unit boundaries were initially drawn and minor pebbles and sedimentary structures were subsequently added. Individual sedimentary units were mainly classified according to grain size range, compaction and sorting. The strike of each section and the selected units was measured with a compass-clinometer. Moraine spacing was estimated in the field from aerial photographs (LiDAR images with a horizontal ground resolution of 2.5 m) The assessment of sedimentary structures (erosional, depositional and deformational features) provided insights into the physical properties of the individual units. Sediments, which shared similar characteristics (regarding grain size, sorting, compaction), were grouped into distinctive lithofacies units

and visualised using a uniform lithofacies code(Krüger and Kjaer, 1999, Fig. 11). The nature of contacts between basal units (gradual or sharp) as well as the visual clast shape and roundness were considered at each exposure.

Only one single dominating lithology (dolomite for the western lateral moraine and micaschist for the eastern lateral moraine) has been sampled. Even if this mix between the lithologies of dolomite and micaschist influences the impact that the lithologies exert on weathering and clast stability (Lukas et al., 2013) this approach was chosen to sample the predominant lithologies of the lateral moraines. The hand-picked clasts of the single sections were compared to own control samples with known transport history (extraglacial, supraglacial, subglacial and fluvial sources). Co-variance plots, displaying angularity indexes (RWR-, RA-, and C_{40}- indices) were used to analyse the clasts' alternating roundness. At first, very stiff, cemented, glaciofluvial gravels were mistaken for true subglacial control samples. But after a thorough re-assessment it turned out to be impossible to safely obtain a subglacial control sample adjacent to the glacier portal (due to crumbling of ice at the glacier margin). Supraglacial control samples were taken on top of the glacier at around 20 m from the glacier portal. Proximal fluvial control samples have been retrieved at a close distance to the glacier portal (at a distance of c. 500 m). Distal fluvial control samples were taken at distances of 1,000 m and 2,000 m downstream. Unfortunately, the nature of the area did not allow to retrieve an extraglacial control sample for the dolomite lithology (the steep walls of the Königspitze were not accessible due to their steepness).

4.3 Clast shape and provenance

The morphology of a clast distinctively reveals its transport, erosional and depositional history (Benn and Ballantyne, 1993). In order to differentiate between single debris transport path histories at Suldenferner well-established methods were considered (Benn and Ballantyne, 1993; 1994; Lukas et al. 2013). The three orthogonal axes (e.g. a, b, c-axes) of 50 clasts per sample were measured with a tape measure in each exposure (within a restricted area of max. 20x20 cm per facies unit). The a-axes of these clasts were sampled within a restricted size range between 3 and 15 cm. These datasets were progressively plotted with a revised version of Tri-Plot (Graham and Midgley, 2000; Lukas et al., 2013). While applying these methods, three possible end members (e.g. blocky, elongated and platy) of a clast could be distinguished (Sneed and Folk, 1958; Fig. 12; Table 2).
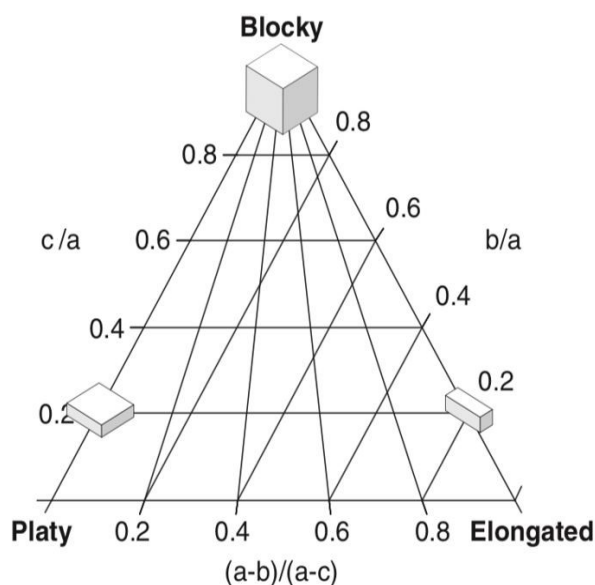

Fig. 12. Clast roundness categories (after Sneed and Folk, 1978)

Table 2. Criteria used to differentiate between single clast roundness classes. Modified after Benn and Ballantyne (1994).

Description	Roundness class
Very acute edges and/or sharp protuberances	Very angular (VA)
Acute edges with no evidence of rounding	Angular (A)
Rounding confined to edges; faces intact	Sub-angular (SA)
Rounding of edges and faces; often facetted	Sub-rounded (SR)
Marked rounding of both edges and faces; marging of edges and faces	Rounded (R)
Distinction between faces and edges not possible	Well-rounded (WR)

5 Results

5.1 Geomorphological Mapping

The foreland of Suldenferner can be divided into three main parts (Fig. 13, Fig. 14): (i) the upper valley (southern rim) with exposures of steep bedrock and the glacial body of the debris-covered glacier Suldenferner; (ii) the central part containing erosional remnants of the lateral moraines, outwash horizons (total area< 20 m²) and outwash terraces (separated by the river Suldenbach, mostly devoid of vegetation); and (iii) a zone of former stagnant ice (undulating terrain), supplemented with areas of alpine mountain vegetation on the northern rim of the study area. The most prominent geomorphological features of the Suldenferner foreland are two outstanding lateral moraines (western and eastern lateral moraines, Table 3). Due to their variable lithological composition (mainly dolomite within the western lateral moraine and mainly micaschist, some dolomite and paragneiss within the eastern lateral moraine) they will be described separately in this thesis (Table 3). The western lateral moraine is accompanied by a set of subsidiary ridges (at the southwestern rim of the study area) and erosional remnants of the lateral moraines. Similarities between the moraines comprise their total length of up to 3 km. The height of the moraines varies locally between c. 110 to 130 measured above ground on the proximal side. Moreover, both lateral moraines decrease in height with increasing distance (i.e. northwards) from the glacier.

5.2 Sedimentology

On the whole, 19 artificial exposures were created by hand in the western lateral moraine. The eastern lateral moraine was assessed in ten hand-created exposures. Fewer sections have been established for the eastern lateral moraine due to a general lack of accessibility (safety reasons). In order to summarise the vast range of field evidence, three representative sections from the western lateral moraine (W-3, W-13 and W-18) and two sections from the eastern lateral moraine (E-3 and E-6) have been established. Moreover, it has to be mentioned that two exposures (M-1, M-2) have been created within the end moraine from 1927 (at the northern rim of former areas of stagnant ice) in order to compare their sedimentological evidence with those of the lateral moraines. Due to similar sedimentological characteristics, data from the 1927 moraine are listed within the table of the western lateral moraine. Further, a synthetic profile log (over 12 m in vertical expansion that covers the accessible parts of the lateral moraine) has been established to put additional emphasis on the development of the western

Table 3. Comparison of the lateral moraines at Suldenferner.

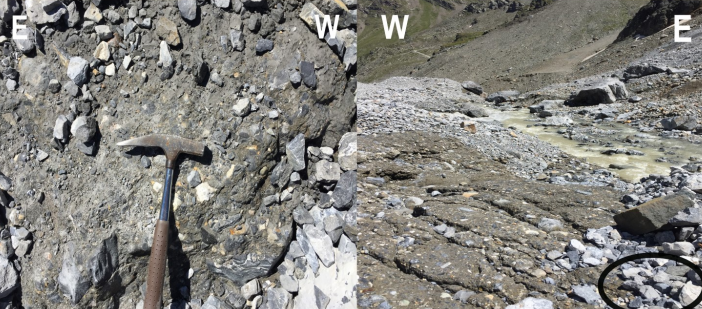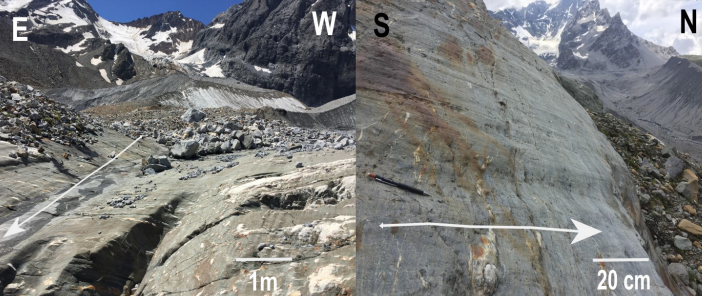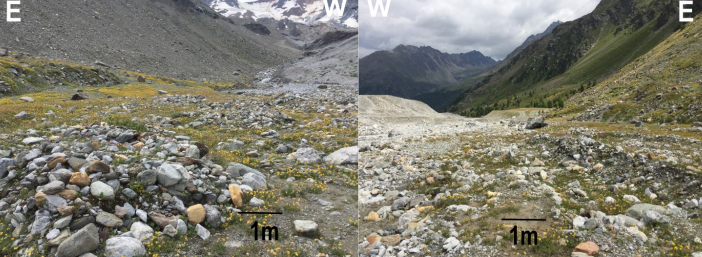|	Western lateral moraine	Eastern lateral moraine
Depth to bedrock	>20 m	>40m
General shape	Southern part (adjacent to the glacier): accompanied by a set of subsidiary ridges that are not directly connected to the main lateral moraine Northern part (distal to the glacier): accompanied by a moraine formed in 1927 (approximately 500 m long, eastwards extending branch)	Singular ridge (linear-slightly parabolic shape)
Crestline	Continuous development (alignment: 80°ENE, 260° WSW)	Artificially altered by a walking path (alignment: 30° NE, 210° SW)
Steepness of slopes	Pronounced steepness of both proximal and distal slopes (locally reaching up to 80°)	Gentle, quite uniform distal slopes (25°-30°), steeper proximal slopes (40°-60°).
Presence of ridge fragments (erosional remnants of the moraines)	Reaching lengths between 10 and 25 m and heights between 15 and 25 m. The fragments are frequently interrupted by small, silted-up depressions and meltwater channels.	✗
Presence of gullies	✓ Proximal and distal slopes intensively gullied	✓ Proximal slopes gullied
Presence of coalescing fans at the base of the moraines	✓ Most frequent in areas close to the glacier portal	✗
Presence of vegetation	✗	✓ Areas colonised by shrubs and grasses at the northern rim of the distal slope

Distribution and description	Photographic field evidence	Elements of mapping
This element is detected close to the glacier portal. It is characterised by a very compact, concrete-like, clast-rich, fine matrix. Water-reworked material (i.e. black circle in figure) accompanies these stiff deposits.		*Subglacially-overridden outwash*
This element is found both proximal and distal to the glacier. It shows clear evidence of striations (e.g. white arrow in figures). Multiple meltwater gullies mark the former water-flow direction.		*Ice-moulded bedrock*
This element is present at the northern rim of the study area. It is characterised by a succession of depressions and elevations (undulating terrain) and contains sorted rings of dolomite (i.e. black circles in figure).		*Former areas of stagnant ice*
This element is present at the north-eastern rim of the study area. It contains the downvalley accumulation of sediments. The element marks the migration of the river Suldenbach.		*Outwash terraces*
These elements are frequent in the center of the study area, adjacent to the western lateral moraine. They appear as linear ridges, with heights > 0.5 m. They are aligned at angles of 50-60° to the former ice-flow direction. (i.e. white arrow in figure).		*Erosional remnants of the lateral moraines*
This element is preserved in the southwest of the study area as steep gullies, reaching several meters of depth (i.e. white lines in figure). It indicates processes of intensive reworking by meltwater streams.		*Gullied glaciogenic material*

Fig. 13. Main elements of geomorphological mapping in the Suldenferner foreland.

19

Glacial Geomorphology of the Suldenferner Foreland, Italy (2019)

Processes of lateral moraine formation at a debris-covered glacier

Legend:

- overhanging rock wall
- gullied glaciogenic material
- subglacially overridden outwash
- proximal lateral moraine
- distal lateral moraine
- bedrock surrounded by scree
- fall sorted scree
- debris-covered glacier
- ice moulded bedrock
- former areas of stagnant ice
- 1927 moraine
- talus slope

- steep bedrock
- paths
- rivers
- moraine crestline
- subaerial meltwater channels

- buildings
- outwash terraces
- outwash horizon
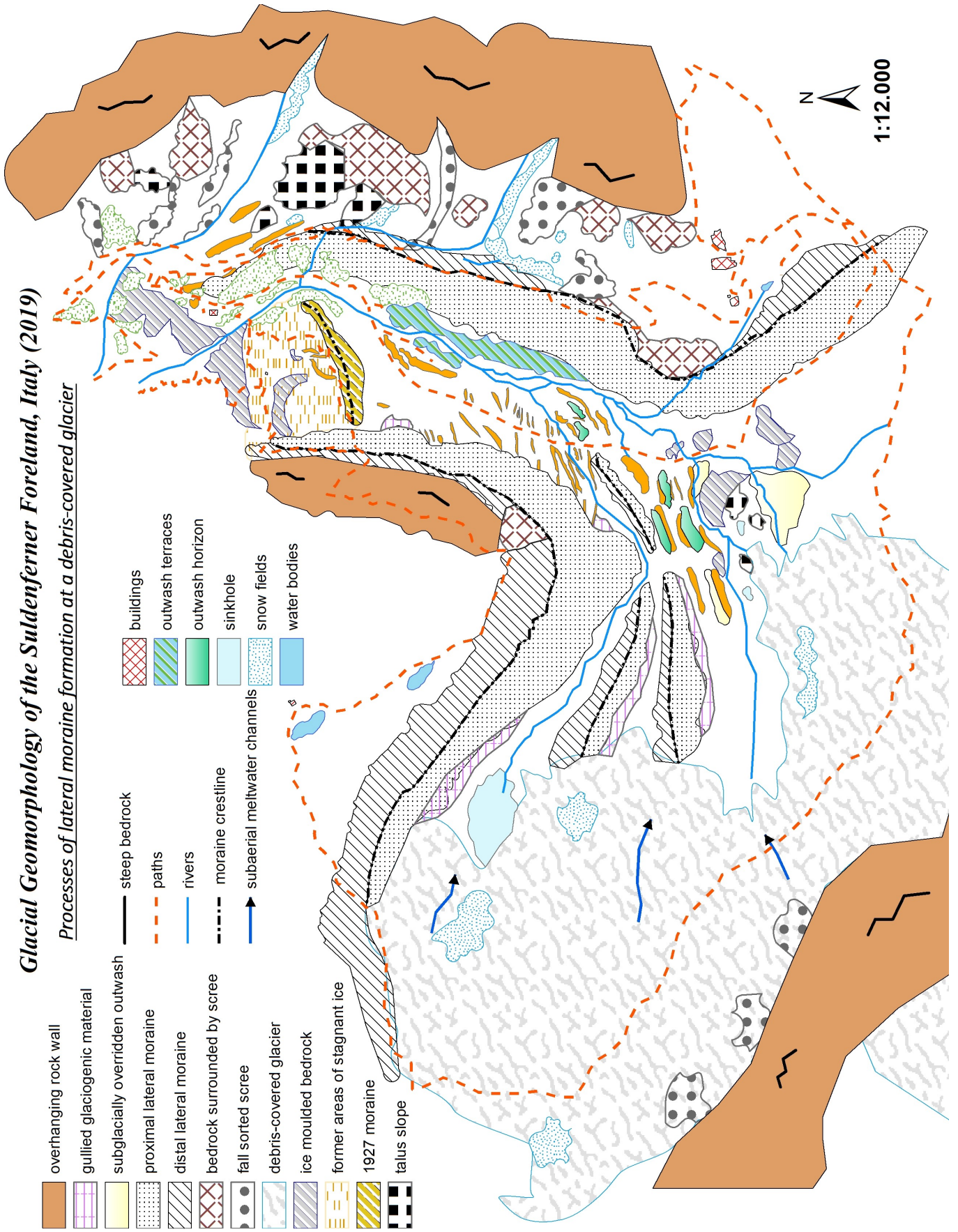- sinkhole
- snow fields
- water bodies

1:12.000

Fig. 14. Glacial geomorphology of the Suldenferner foreland. Scale 1:12,000.

Table 4. Overview of the sedimentological characteristics of the western lateral moraine at Suldenferner. Section numbers in bold (type localities) are representative of *LFA 1* and *LFA 2*, respectively. Clast shape measurements were effected on 50 clasts per section. Exposures within the 1927 moraine are listed on the bottom of the table (M-1 and M-2).

Section no.	Coordinates	Altitude (m)	Lithofacies recorded	Lithofacies association	RWR (shape)	C_{40} (shape)	RA (shape)
W-1	46°29`41``N, 10°35`09``E	2515	DgFm$_2$-2, Gh, GRm	LFA 2	0	42	82
W-2	46°29`40``N 10°35`12``E	2528	DgFm$_2$-2, Go, GRm	LFA 2	0	44	78
W-3	46°29`40``N 10°35`13``E	2478	DmCc-2, Go, Fm	LFA 1	0	50	62
W-4	46°29`41``N 10°35`18``E	2433	DhMm$_3$-2, Gh, GRm, Sm, Fm	LFA 2	0	30	60
W-5	46°29`34``N 10°35`10``E	2410	DgFm$_2$-2, Gh, GRm	LFA 2	2	64	56
W-6	46°29`30``N 10°35`02``E	2302	DhMm$_3$-2, Go, GRm	LFA 2	0	56	68
W-7	46°29`36``N 10°35`02``E	2435	DhMm$_3$-2,Gh, GRm	LFA 2	0	36	58
W-8	46°29`35``N 10°35`06``E	2425	DhMm$_3$-2,Gh, Gro	LFA 2	0	78	64
W-9	46°29`31``N 10°35`10``E	2335	DhMm$_3$-2, Gro, Sm	LFA 2	0	72	62
W-10	46°29`33``N 10°35`03``E	2315	DhMm$_3$-2, Gh, Grm, Sm, Fm	LFA 2	0	42	60
W-11	46°29`33``N 10°35`04``E	2305	DmCc-2, Gh, Go, Fm	LFA 2	0	40	16
W-12	46°29`33``N 10°35`08``E	2303	DhMm$_3$-2, Go, GRm	LFA 1	0	52	54
W-13	46°29`34``N 10°35`19``E	2362	DgFm$_2$-2, Gh, Go, GRm, Sm, Fm	LFA 2	0	52	76
W-14	46°29`36``N 10°35`24``E	2345	DgFm$_2$-2, Gh, Go	LFA 2	0	44	60
W-15	46°29`35``N 10°35`24``E	2356	DgFm$_2$-2, Gh	LFA 1	0	52	76
W-16	46°29`37``N 10°35`28``E	2360	DhMm$_3$-2, Gh,Go,GRm, Sm, Fl	LFA 1	0	68	48

Table 4. Continued

W-17	46°29`58``N 10°35`31``E	2297	DgFm$_2$-2, Gh, Go, GRm	LFA 2	0	56	62
W-18	46°29`59``N 10°35`40``E	2313	DmCc-2, Go	LFA 2	0	64	62
W-19	46°29`59``N 10°35`43``E	2297	DgFm$_2$-2, Gh, Go	LFA 1	0	64	62
M-1	46°29`45``N 10°35`15``E	2465	DhMm$_3$-2, Go, GRm	LFA 2	0	64	28
M-2	46°29`44``N 10°35`18``E	2436	DgFm$_2$-2, Gh, Go, GRm	LFA 2	0	66	28

Table 5. Roundness data (RWR-index, C$_{40}$-index, RA-index) of the western lateral moraine crestline samples (containing 50 clasts per sample). Crestline samples on top of the 1927 moraine are labelled as M-a and M-b, respectively.

Label	Coordinates	Altitude (m)	RWR (shape)	C$_{40}$ (shape)	RA (shape)
W-a	46°29`44``N; 10°35`10``E	2582	0	66	84
W-b	46°29`43``N; 10°35`23``E	2575	0	50	82
W-c	46°29`42``N; 10°35`16``E	2563	0	36	82
W-d	46°29`42``N; 10°35`18``E	2565	0	34	66
W-e	46°29`36``N; 10°35`05``E	2425	0	36	60
W-f	46°29`35``N; 10°35`09``E	2415	0	32	34
W-g	46°29`32``N; 10°35`06``E	2385	0	70	86
W-h	46°29`58``N; 10°35`31``E	2395	0	56	70
W-i	46°29`58``N; 10°35`31``E	2386	0	28	100
W-j	46°29`58``N; 10°35`31``E	2375	0	28	68
W-k	46°30`00``N; 10°35`37``E	2260	0	58	62
W-l	46°30`01``N; 10°35`45``E	2325	0	70	84
M-a	46°29`32``N; 10°35`12``E	2383	0	70	86
M-b	46°29`37``N; 10°35`27``E	2383	0	48	62

lateral moraine.

5.2.1 Western Lateral Moraine

The sedimentological characteristics of the sections and the clast roundness data of the crestline samples are depicted in Tables 4 and 5, respectively. The pebbles and boulders within all sections of the western lateral moraine are exclusively of dolomite lithology.

5.2.1.1 Lithofacies association 1

LFA 1 comprises a graded, friable, matrix-supported diamicton (DgMm$_2$-2) which is characterised by medium-grained, silty-sandy matrix (Fig. 15). In general, the sediments within lithofacies 1 are of diamictic nature, supplemented with minor sequences of sorted sediments. Lithofacies 1 is most significantly representative of section W-3. This section is situated at an altitude of 2365 m on the main branch of the western lateral moraine, approximately 30 m below the moraine crestline. The section is orientated at 085° and runs parallel to the moraine crestline. The majority of the clasts which are present within the diamictic matrix are characterised by average a-axes between 10 and 15 cm. Three bodies of openwork gravel (Go) and one body of horizontally-bedded gravel (Gh) appear randomly dispersed across the section (Fig. 15a). The most significant body of openwork gravel (Go) is identified at the bottom of the section, reaching a horizontal expansion of 80 cm. Another striking feature of the exposure comprises nine distinctive bodies of fines (Fm). The biggest body of these sorted sediments is detected between 0.75 and 1.3 m of section thickness (dimensions: 20 x 15 cm). The majority of the clasts which have been excavated are angular (80%) and subangular (20%). One pebble is characterised by facets, while the remaining clasts lack striae. Moreover, none of the clasts exhibits a bullet-shaped morphology. Lithofacies 1 was detected in sections W-3, W12, W-15, W-16 and W-19 on the proximal side of the western lateral moraine. Lithofacies 1 was also attributed with the sediments of exposures within the 1927 moraine (M-1 and M-2).

5.2.1.2 Lithofacies association 2

LFA 2 is characterized by a massive, homogeneous, fine-grained, clayey-silty diamiction (DgFm2-2) that is friable and easy to excavate. Lithofacies 2 represents a fine-grained, clayey- silty, graded diamicton (DhMm3-2). Being the most frequent lithofacies at Suldenferner, lithofacies 2 is described by two sections (W-13 and W-18).

Section W-13 (Fig. 16) is situated at an altitude of 2305 m on the distal side of the western lateral moraine. It is found in a gully wall and located parallel to (and 10 m below) the moraine crestline. The orientation of the section is at 275°. The diamicton (DgFm22) is crudely stratified and dips between 40 and 45° away from the glacier. Distinctive bodies of gravel (two bodies of horizontally-bedded gravel, Gh, and four bodies of openwork gravel, Go) appear parallel to the stratification (Fig. 16a). The most prominent body of openwork gravel (Go) is identified at the bottom of the exposure (analogous to section W-3), reaching dimensions of 80 x 35 cm. Further, two lenses of massive granule gravel (GRm) are located in the upper parts of the section and are variably distributed between multiple clast agglomerations. The section also contains one intercalated lense of medium-grained sand (Sm) that is found close to the center of the section. The sorted sediments are characterised by dimensions of 10 x 5 cm and lack any deformational structures. Moreover, one body of massive fines is found close to the bodies of openwork gravel (dimensions: 5 x 5 cm). The biggest clasts that are present within the diamicton are characterised by maximum a-axes between 15 and 25 cm. These clasts show a clear alignment to the proximal side of the western lateral moraine. After removal, the clasts do not leave observable imprints in the matrix. This suggests a low consolidation of the sediments. Most of the clasts that are present within the matrix are angular (63%) and subangular (37%). Two clasts are bullet-shaped and none of them is characterised by facets or striae. The top of the moraine crestline is defined by an agglomeration of angular boulders with a-axes > 10 cm.

Section W-18 (Fig. 17) is located at an altitude of 2360 m on the proximal side in a subsidiary branch of the western lateral moraine. The exposure is localised approximately 25 m below the moraine crestline and aligned parallel to it (orientation of 070°). The diamicton (DhMm3-2) that characterises the outcrop is classified as matrix-supported, clast-rich and slightly harder to excavate as compared to the diamicton of section W-13 (DgFm2-2). The bottom parts of the exposure are characterised by an elliptical body of openwork gravel (Go) that reaches dimensions of 110 x 30 cm. Two elliptical lenses of medium–grained sand (Sm) are found sandwiched between an agglomeration of clasts at the center of the exposure (dimensions: 8 x 5 cm). Moreover, three bodies of massive fines (Fm) and one lense of laminated fines (Fl) are found in the upper part of the exposure (from 0.5 m of section thickness). The most prominent lense of fines reaches a horizontal extension of 50 cm. In contrast to section W-13, section W-18 does not show any clear evidence of stratification (Figure 18a). Moreover, bodies of gravel (mostly openwork gravel, Go) and massive granule gravel (GRm) are present. These bodies reach maximum thicknesses of 35 cm.
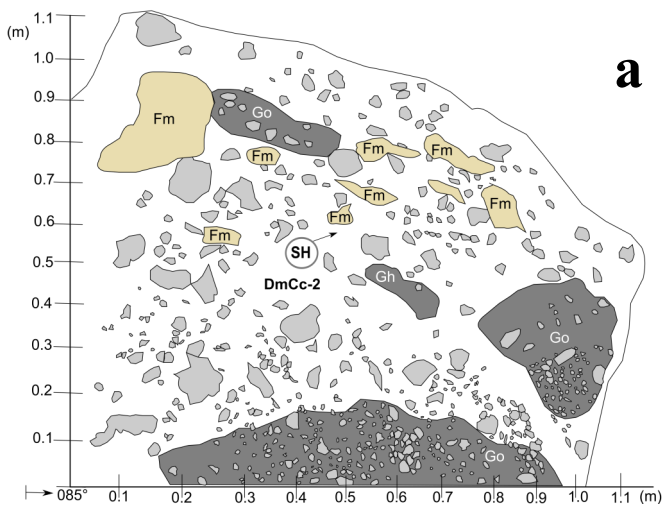
Fig. 15. (a) Sedimentary log of section W-3, representing *LFA 1*. (b) Close-up photograph of section W-3.
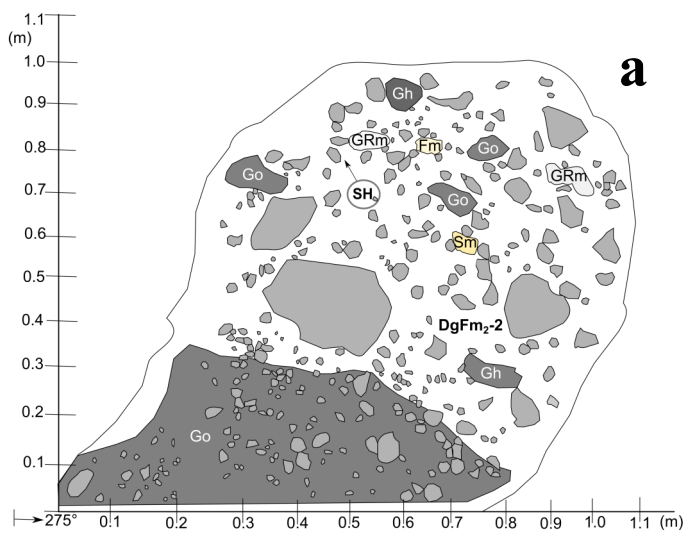

Fig. 16. (a) Sedimentary log of section W-13, representing *LFA 2*. (b) Close-up photograph of section W-13.
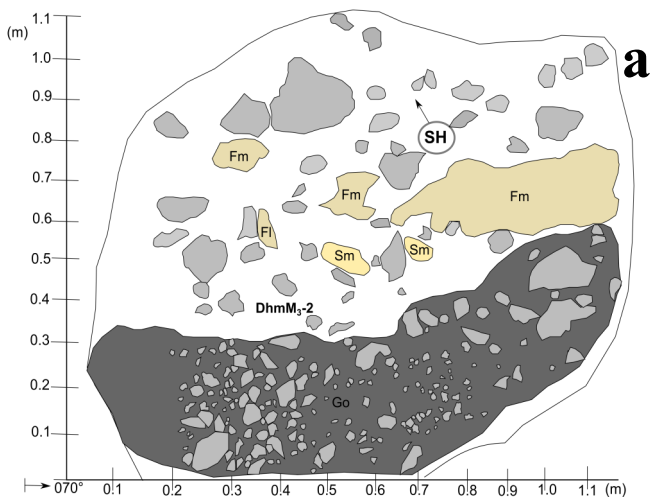

Fig. 17. (a) Sedimentary log of section W-18, representing *LFA 2*. (b) Close-up photograph of section W-18.

24

Fig. 18. Close-up photograph of laminated sand, approximately 5 m eastwards of section W-18.

Four lenses of medium-grained, massive sand (Sm) that each reach widths up to 20 cm are observable. These lenses are dipping 20°-25° northeastwards. Further, a 15 cm wide body of laminated sand (Sl) is detected at a distance of approximately 5 m to section W-18 (Fig. 18). Lithofacies 2 was discovered in four exposures (W-7, W-11, W-18, W-19) on the distal side and nine sections (e.g. W-1, W-2, W-4, W-8, W-9, W-10, W13, W-14, W-17) on the proximal side of the western lateral moraine. It is also attributed with the sediments within the 1927 moraine (M-1, M-2).

5.2.1.3 Representative Profile Log

In order to accurately quantify the sedimentological characteristics of the western lateral moraine, a representative profile log of 12 m in vertical expansion has been established (Fig. 19). Because the main branch of the western lateral moraine was hardly accessible it was decided to establish the log in a gully wall that runs parallel to the moraine crestline (due to steep slopes and overhanging boulders, safety reasons). The evidence that is contained within the log will provide further clues about the genesis of the lateral moraines at Suldenferner. The log mainly represents the sediments of sections W-8, W-9 and W-10. These sections are located on the proximal side in a subsidiary branch of the western lateral moraine. The base of the log is set at exposure W-10, at an altitude of 2315 m. The predominant grain size of the log is set as boulders, representing mostly heterogeneous, medium-grained, silty-sandy diamictons (n=6, code: D1). Only two diamictons (with bases at unit thicknesses of 1.6 and 8.6 m above ground, respectively) deviate from the main trend, containing lenses of silt (D1-si) and lenses of medium grained sand (D1-s). Two massive diamictons (D2) appear at unit thicknesses of 3.2 and 4.5 m, respectively. These single diamictons are up to 1.0 m high. Apart from the diamictons, single lenses of sediments (characterised by different dominant grain sizes) are present in the log. A total of three units, containing portions of gravel, granule gravel and medium-grained sand (code: G1) appear at unit thicknesses of 1.1 m, 6.1 m and 9.6 m, respectively. Further, a total of two mixed sequences (containing gravel and granule gravel, code: G2) are detected at unit thicknesses of 4.1 m and 10.6 m, respectively. Another interesting feature of the log is marked by a succession of silt and fines (code: F1), at 2.5 m unit thickness above ground. It is observable that the boundary between the superimposed units is commonly wavy-undulating.
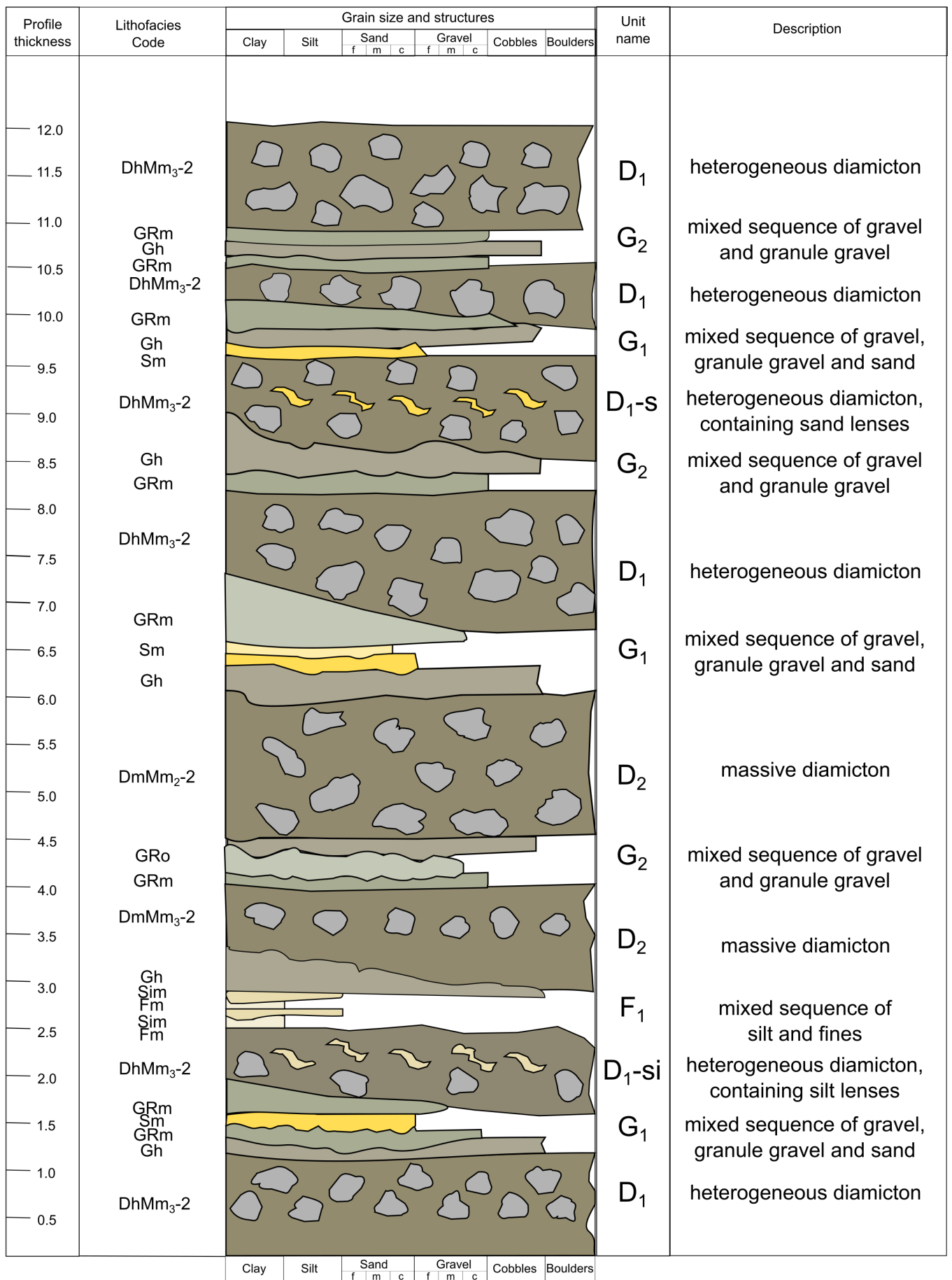
25

Profile thickness	Lithofacies Code	Grain size and structures							Unit name	Description
		Clay	Silt	Sand (f, m, c)	Gravel (f, m, c)	Cobbles	Boulders			

Profile thickness	Lithofacies Code	Unit name	Description
12.0 – 11.5	DhMm₃-2	D_1	heterogeneous diamicton
11.0 – 10.5	GRm / Gh / GRm	G_2	mixed sequence of gravel and granule gravel
10.5	DhMm₃-2	D_1	heterogeneous diamicton
10.0 – 9.5	GRm / Gh / Sm	G_1	mixed sequence of gravel, granule gravel and sand
9.0	DhMm₃-2	D_1-s	heterogeneous diamicton, containing sand lenses
8.5	Gh / GRm	G_2	mixed sequence of gravel and granule gravel
8.0 – 7.5	DhMm₃-2	D_1	heterogeneous diamicton
7.0 – 6.5 – 6.0	GRm / Sm / Gh	G_1	mixed sequence of gravel, granule gravel and sand
5.5 – 5.0	DmMm₂-2	D_2	massive diamicton
4.5 – 4.0	GRo / GRm	G_2	mixed sequence of gravel and granule gravel
3.5	DmMm₃-2	D_2	massive diamicton
3.0 – 2.5	Gh / Sim / Fm / Sim / Fm	F_1	mixed sequence of silt and fines
2.0	DhMm₃-2	D_1-si	heterogeneous diamicton, containing silt lenses
1.5	GRm / Sm / GRm / Gh	G_1	mixed sequence of gravel, granule gravel and sand
1.0 – 0.5	DhMm₃-2	D_1	heterogeneous diamicton

Fig. 19. Representative profile log established in a subsidiary branch of the western lateral moraine.

The sharp borders between the successions of horizontally bedded gravel (Gh) and massive granule gravel (GRm) between 10.5 and 11 m of unit thickness above the ground mark an exception to this rule. Most of the single units are horizontally oriented. However, some of the units dip slightly towards northeast (075°), at angles between 10 and 15° (i.e. horizon D1 at 7.5 m of unit thickness above ground). It turns out that most of the diamictic units are superimposed by sequences of horizontally-bedded gravel (Gh), massive (GRm) and openwork (GRo) granule gravel.

5.2.2 Eastern Lateral Moraine: Lithofacies association 3 (LFA 3)

The eastern lateral moraine was assessed with a total of ten exposures (Table 6). It has to be mentioned that sections were only dug in the proximal side of the eastern lateral moraine. This is because the distal slopes of the eastern lateral moraine are densely vegetated on the northern edge of the moraine.

In contrast to the western lateral moraine, the eastern lateral moraine is more homogeneous in nature and characterised by only one predominant lithofacies (*LFA 3*). However, this homogenity does not regard the lithology of the clasts incorporated within the diamictic matrix, as clasts of micaschist, dolomite and paragneiss prevail. Clast shape measurements were carried out on clasts of micaschist, the predominant lithology within the eastern lateral moraine. However,

it is striking that the biggest clasts within all the exposures at the eastern lateral moraine are of dolomite lithology. The sedimentological features of the sections of the eastern lateral moraine and clast roundness data of the crestline samples are depicted in Table 6 and Table 7, respectively. It turns out that the individual sections of the eastern lateral moraine are characterised by similar sediments and well-comparable sedimentary structures.

LFA 3 is described from both sections E-3 and E-6. Section E-3 (Fig. 20) is located at an altitude of 2364 m on the proximal side of the eastern lateral moraine, approximately 2 m below the moraine crestline. The section is aligned parallel to the crestline of the eastern lateral moraine and oriented 210° SE. Section E-3 mainly consists of a massive, homogeneous, coarse-grained (sandy-gravelly) diamicton (DmCm$_1$-1) that is matrix-supported and loose (easy to excavate) with a moderate amount of clasts. Two lenses of granule gravel (massive, GRm, and openwork, GRo) appear randomly dispersed over the whole section (Fig. 20a). A total of three lenses of medium-grained sand (reaching maximum horizontal expansions of 10 cm) are present in the upper part of the exposure (from 0.5 m upwards). These individual beds of medium-grained sand are intercalated and resemble flame structures. Further, a total of seven bodies of massive fines appear randomly dispersed across the exposure (dimensions: 7 x 5 cm). The biggest boulders within the section

Table 6. Roundness data (RWR-index, C$_{40}$-index, RA-index) of the eastern lateral moraine crestline samples (total of 50 clasts in each exposure).

Sample	Coordinates	Altitude (m)	RWR (shape)	C$_{40}$ (shape)	RA (shape)
E-a	46°29`14``N	2628	0	98	80
	10°35`56``N				
E-b	46°29`20``N	2620	0	92	78
	10°35`50``N				
E-c	46°29`22``N	2605	0	94	84
E-d	46°29`42``N	2374	0	30	60
E-e	46°29`48``N	2330	0	94	76
E-f	46°29`50``N	2305	0	86	70

Table 7. Overview of the sedimentological characteristics of the eastern lateral moraine at Suldenferner. Clast shape measurements were effected on 50 clasts per exposure. Section numbers in bold are representative of *LFA 3*.

Section no	Coordinates	Altitude (m)	Lithofacies recorded	Lithofacies association	RWR (shape)	C_{40} (shape)	RA (shape)
E-1	46°29`39``N 10°35`49``E	2515	DmCm$_1$-1, GRm	LFA 3	0	78	82
E-2	46°29`40``N 10°35`46``E	2325	DmCm$_2$-1. GRm, Sm	LFA 3	0	74	80
E-3	46°29`42``N 10°35`41``E	2364	DmCm$_1$-1, GRm, Sm, Fm	LFA 3	0	66	76
E-4	46°29`45``N 10°35`49``E	2330	DmCm$_1$-1, GRo, Sm	LFA 3	0	64	84
E-5	46°29`46``N 10°35`51``E	2340	DmCm$_2$-1, GRm, Sm	LFA 3	0	70	92
E-6	46°29`49``N 10°35`52``E	2331	DmCm$_2$-1, GRo, GRm, Sm, Fm	LFA 3	0	66	70
E-7	46°29`50``N 10°35`54``E	2318	DmCm$_1$-1, GRm, Sm	LFA 3	0	72	92
E-8	46°29`51``N 10°35`54``E	2318	DmCm$_2$-1, Sm	LFA 3	0	84	82
E-9	46°29`53``N 10°35`54``E	2318	DmCm$_1$-1, Sm, Fm	LFA 3	0	72	84
E-10	46°30`00``N 10°35`59``E	2266	DmCm$_2$-1, Sm, Fm	LFA 3	0	74	78

(lithology: dolomite) reach a-axes of 25 cm. In contrast, clasts of micaschist are characterised by maximum a-axes of 10 cm. Clast shape measurements reveal three different categories of incorporated clasts: angular clasts (85%), subangular clasts (10%) and very angular clasts (5%).   Section E-6 (Fig. 21) is situated at an altitude of 2331 m on the proximal site of the eastern lateral moraine, approximately 3 m below the moraine crestline. The section runs parallel to the moraine crestline and is oriented at 205° SE.   The diamicton that characterises the outcrop is analogous to that in section E-3 (DmCm$_2$-1). Four lenses of granule gravel (massive, GRm, and openwork, GRo) are in the central part of the section (Figure 20a). The lower lense at 35 cm of section thickness is massive, whereas the remaining lenses display openwork gravel (Go). The section contains more clasts of dolomite as compared

to section E-3. The upper left corner of the section is characterised by two ellipses of medium-grained sand (Sm), that reach dimensions of 15 x 8 cm. A smaller body of medium grained sand (dimensions: 5 x 3 cm) is found interlocked between an agglomeration of dolomite clasts at 0.13 m of section thickness. Seven bodies of massive fines (Fm) are randomly dispersed across the section (dimensions: 3 x 5 cm). Most of the pebbles that have been discovered within the section are angular (90%) and very angular (10%). The boulders that drape the moraine crestline (both micaschist and dolomite) are characterised by maximum a-axes of 20 cm.

5.3 Clast Shape

Clast shape measurements of the individual sections are depicted in Fig. 22 (western lateral moraine) and Fig. 23 (eastern lateral moraine), respectively. Clasts
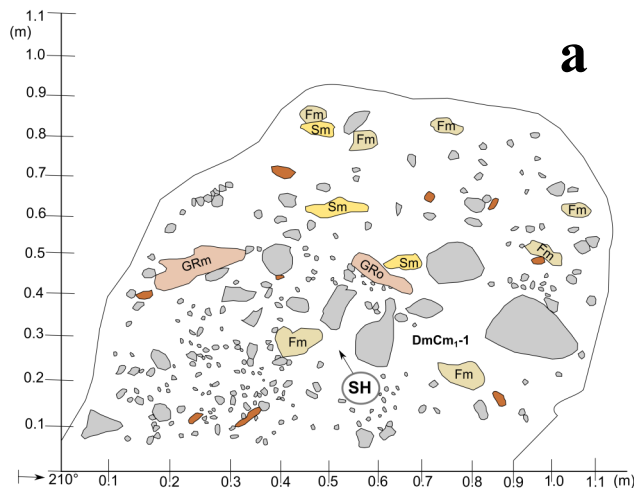
Fig. 20. (a) Sedimentary log of section E-3, representing *LFA 3* (b) Close-up photograph of section E-3.
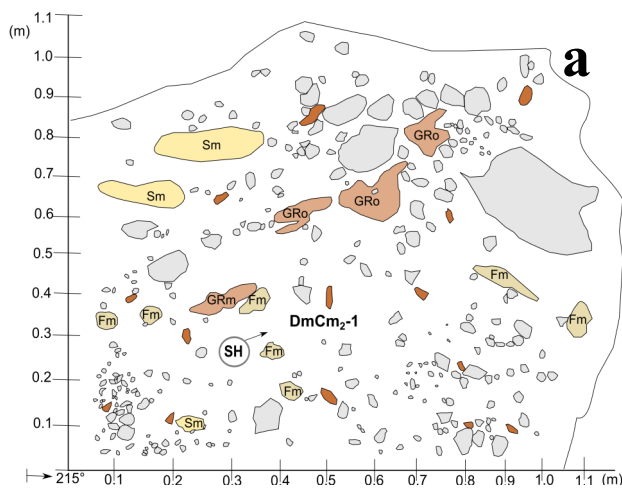

Fig. 21. (a) Sedimentary log of section E-6, representing *LFA 3* (b) Close-up photograph of section E-6.

roundness was also assessed at the crestline of both the western (14 samples) and eastern (nine samples) lateral moraines. The combined datasets show that the lithologies of dolomite (western lateral moraine) and micaschist (eastern lateral moraine) have to be distinguished for effecting accurate clast shape analysis.

5.3.1 Western Lateral Moraine

While comparing section samples with control samples (lithology: dolomite and micaschist) it turns out that the samples plot between the fluvial and supraglacial control envelope (Fig. 22b). It is striking that the range of variation of the single samples is wide, highlighting their variable character. Therefore, it is apparent that the samples are neither truly supraglacial nor fluvial and must display a complex history (potential mix between subglacial, fluvial and englacial transport pathways). The samples are characterised by an average C_{40}-index of 61%, RWR-indices of 0% and RA-indices of 50%. Apparently, the foreland (surface) sample is characterised by a high RA-index of 85%. However, this value is still below the one of the supraglacial control sample (ranging between 90%-

100%). The fluvial control samples show the highest RWR-index (1% - 2%) as well as the lowest C_{40}-index (between 50% and 60%). This circumstance is observable for both the section samples and the crestline samples of the western lateral moraine. It turns out that platiness (C_{40}-index) and angularity (RA/RWR-indices) are nearly equally-well suited discriminators of clast shape (cf. Lukas et al., 2013).

5.3.2 Eastern lateral moraine

In general, the sections of the eastern lateral moraine are characterised by plots between the supraglacial and extraglacial control envelopes (Fig. 23b). The samples that have been obtained from the crestline of the eastern lateral moraine plot closely to the extraglacial control envelope (Fig. 23c). Very angular clasts occur almost exclusively in the sections at the northern rim of the eastern lateral moraine (accompanied by the highest percentage of angular clasts). Further, very angular clasts are abundantly present on the crestline of the eastern lateral moraine, accompanied by a high degree of angular clasts. Micaschist clasts are charac-
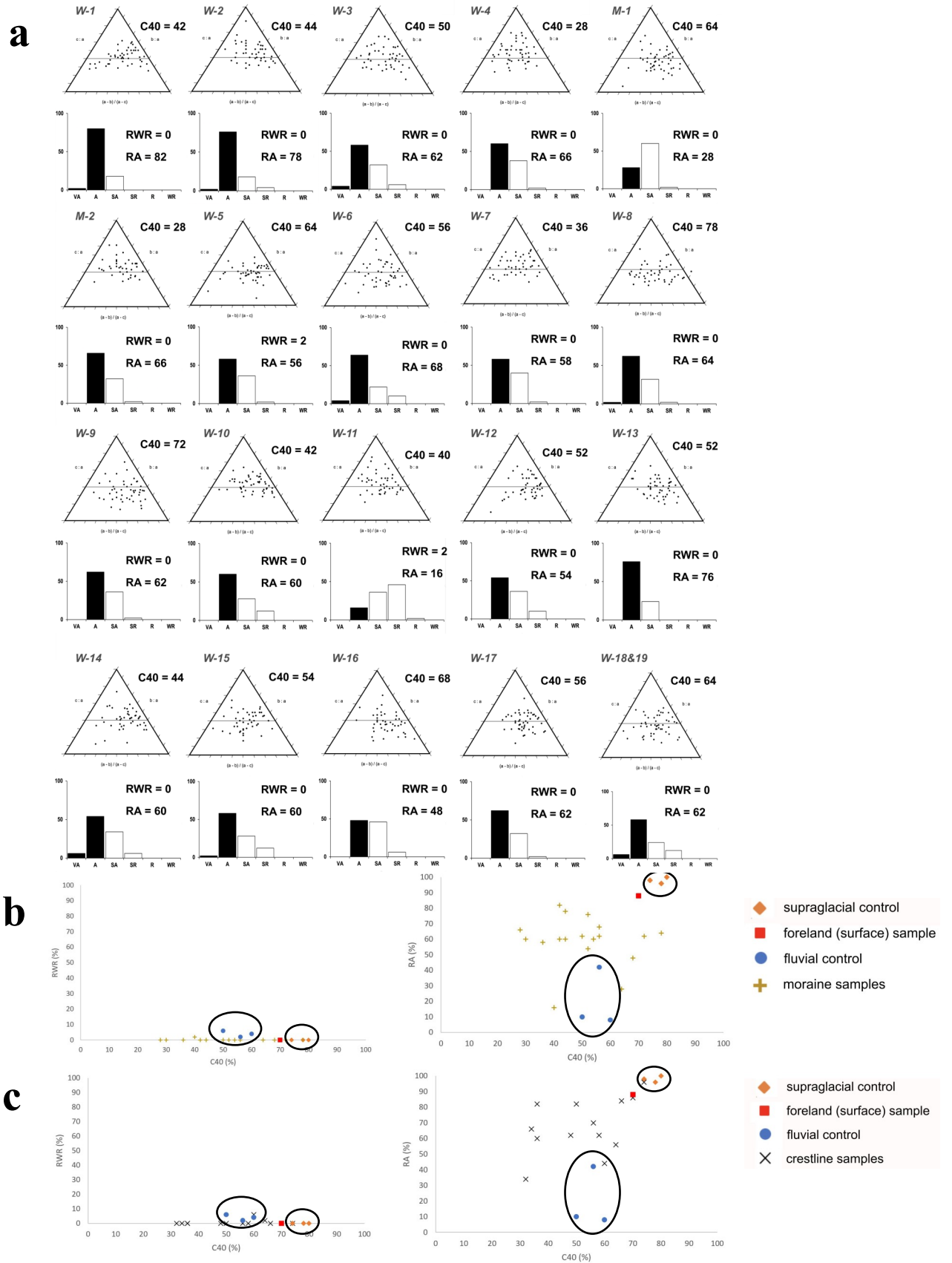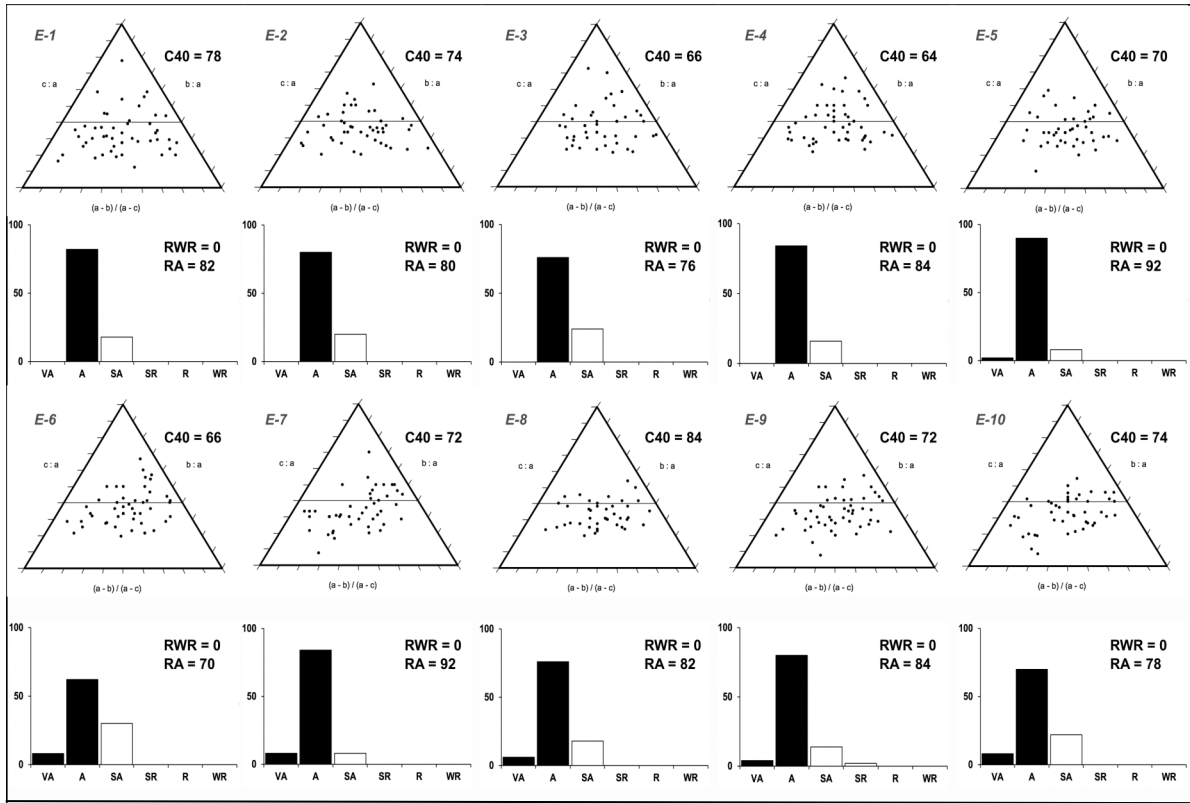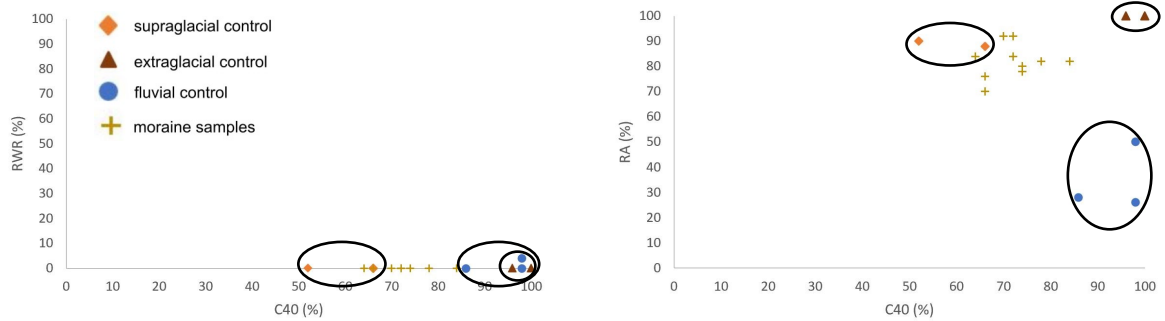
29

Fig. 22. (a) Ternary diagrams and histograms of the western lateral moraine, showing clast form and roundness data, respectively. (b) Co-variance plot comparing *fluvial* and *supraglacial* with **section samples** of unknown origin (RWR-index versus C_{40}-index, RA-index versus C_{40}-index). (c) Co-variance plot comparing *fluvial and supraglacial* samples with **crestline samples** (RWR-index versus C_{40}-index, RA-index versus C_{40}-index).
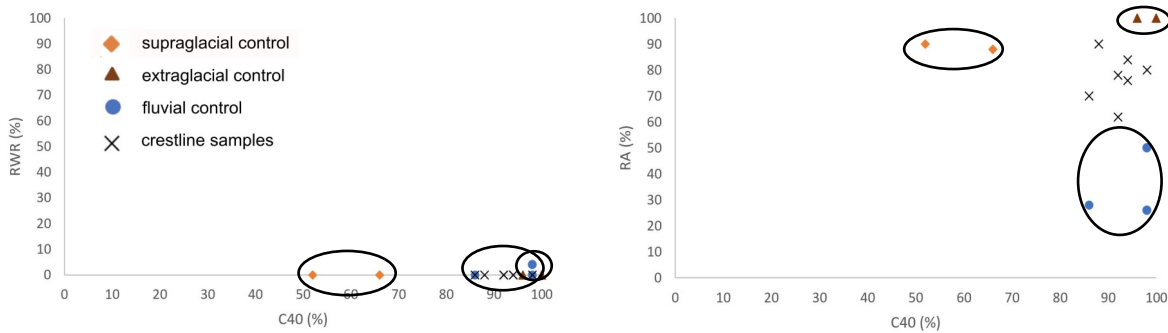
Fig. 23. (a) Ternary diagrams and histograms of the eastern lateral moraine, showing clast form and roundness data, respectively. (b) Co-variance plot comparing *fluvial, supraglacial* and *extraglacial* control samples with **section samples** of unknown origin (RWR-index versus C_{40}-index, RA-index versus C_{40}-index). (c) Co-variance-plot comparing the same control samples with **crestline samples** (RWR-index versus C_{40}-index, RA-index versus C_{40}-index).

31

terised by a generally high anisotropy (resulting in a platy shape) and medium hardness. The extraglacial control envelopes are characterised by a high C_{40}-index (between 95 and 100%). This observation specifically concerns the moraine crestline samples. Contrarily, the supraglacial envelopes generally show medium C_{40}-indices (between 52% and 68%). Surprisingly, both extraglacial and fluvial samples are characterised by comparable RWR–indices (between 0% and 1%). Moreover, it is quite unusual that the fluvial control samples plot very close to the extraglacial control envelope (Lukas et al., 2013). Indeed, the fluvial control envelope is characterised by high C_{40}-indices between 85% and 100%. It turns out that RA-indices are highest for the extraglacial control (98%-100%), and lowest for the fluvial control (25%-45%). Regarding morphological characteristics the results show that only a negligible amount of clasts with facetts (2%) is present within the sections of the eastern lateral moraine. Further, a total lack of striated, and bullet-shaped clasts was noted. It also turns out that the extraglacial samples are more angular than the supraglacial samples (higher RA-index). Further, the results indicate that the supraglacial samples are affected by a decrease in C_{40}-indices, while being quite angular. The micaschist samples obtained from the eastern lateral moraine show a clearer imprint of the processes that control the samples' shapes as compared to the samples of the western lateral moraine. This is mainly, because the samples plot in a scattered pattern and indicate that roundness (i.e. RA-index) is the dominant discriminator of clast shape (cf. Lukas et al., 2013).

The angularity trend of clasts that have been retrieved at the moraine's crestlines differs between the western and eastern lateral moraines (Fig. 24). It turns out that dolomite clasts on top of the western lateral moraine (Fig. 25) develop from angular to subangular clasts with increasing distance to the glacier, whereas the eastern lateral moraine (Fig. 26) is more homogeneous in nature, characterised by mainly angular clasts on the moraine's crestline (exception: sample E-f with a high amount of very angular clasts).

6 Discussion

In order to reconstruct the mechanisms of lateral moraine formation at Suldenferner, the genetic processes are firstly assessed from a sedimentological point of view. Thereafter, moraine morphology, preservation potential and stability will be presented. Further, a comparison with previous case studies on lateral moraines in high-alpine settings will be conducted in order to put the results into a broader sedimentological context. Limitations and implications for future studies will also be encountered, until finally establishing a conceptional model of lateral moraine formation at the high-alpine, debris-covered glacier Suldenferner.

6.1 Moraine distribution and sedimentology

6.1.1 Western Lateral Moraine

6.1.1.1 Lithofacies association 1 (LFA 1)

The sediments that are contained within *lithofacies association 1* are of diamictic nature, supported by occasional gravel bodies. Due to their coarse texture (high percentage of clasts dispersed within the matrix) and a trend towards subangular clasts (experiencing fluvial rounding) they are interpreted as reworked glaciofluvial deposits (Lukas et al., 2012). The fact that the sediments are friable and easy to excavate suggests deposition from a subaerial setting (Boulton and Eyles, 1979). It is possible that these sediments represent short-lived depositions in small rills and swings between gravitational and fluvial processes (Boulton and Eyles, 1979). Grain size variations and changes in sorting reflect changes in flow velocity (Benn et al., 2003; Benn and Evans, 2010). The sediments that are integrated into the main moraine corpus are water-saturated during the ablation season and finally deposited as gravity flows (Benn et al., 2003; Tonkin, 2016). Contemporarily, shallow sheet flows are generated along the ice margin, forming ice-contact fans (Lukas et al., 2012). Occasional debris layers accumulate between the glacier and the proximal flank of the western lateral moraine, further contributing to moraine stability (cf. Boulton and Eyles, 1979, Lukas et al., 2012). The deposits of *lithofacies association 1* accompany ice-marginal stacks of supraglacially-derived debris flows that form near-symmetrical lateral moraines (Lukas et al., 2012; McMahon, 2015). The presence of openwork gravel in the exposures indicates reworking of an englacial fluvial sediment that has emerged from an englacial conduit fill (cf. Aber and Krüger, 1999; Lukas and Sass, 2011; McMahon, 2015). Moreover, a series of coalescing fans form ramps at the angle of repose (especially in the western corner of the study area, where the moraines were hardly accessible). These fans - reaching steep angles between 60° and 70° - are similar to ice-marginal features that were assessed at Findelengletscher (Lukas et al., 2012). Further, the proximal side of the western lateral moraine represents an ice-contact face, where the material is at the angle of repose (Curry et al., 2009).

6.1.1.2 Lithofacies association 2 (LFA 2)

Lithofacies association 2 mostly occurs in the uppermost, distal parts of the western lateral moraine. The diamictons of *LFA 2* are conformably arranged and show gradual (not sharp), non-erosional contacts. The fact that *LFA 2* comprises sorted sediments (being present parallel to the moraine crestline) suggests that it represents debris flows that have been deposited

from subaerial position (Benn et al., 2003). Indeed, the sediments are interpreted as localised, reworked material of underlying debris flows (Benn et al., 2003). The internal stratification of the sediments indicates deposition from a slow flow (Benn et al., 2003, Reinardy and Lukas, 2009). Further evidence in support of this interpretation is provided by the parallel alignment of clasts (with clast axes mainly dipping away from the glacier). The diamictons that appear close to the moraine surface are regarded as products of multiple processes. They are regarded as products of debris flows that have been deposited either (i) during rainfall events, suggesting that the units of sorted sediments derive from an alternating amount of meltwater in the system (Boulton and Eyles, 1979) or (ii) after the glacier has retreated from its position and withdrawn its support at the proximal face (Lukas et al., 2012). It is probable that the proximal units of the moraines collapsed after glacial retreat. Processes of sliding and reworking (Benn and Evans, 2010) also have to be taken into account. It is presumable that the consolidation of the proximal slopes of these lateral moraines was further aided by lateral drag (Curry et al., 2009). Both stratified diamictons and sequences of openwork gravel (Go) are found in proglacial, ice-marginal settings. Processes of sediment deposition are accompanied by a terrestrial, ice-contact fan formation (Benn et al., 2003). The sedimentary bedding within the moraines is rather intact than disrupted. This could be indicative of either an absence of deformation during emplacement or a preservational vanish of deformational structures due to the coarse texture of the sediments (Patterson and Cuffey, 2010; Evans et al., 2010).

According to clast shape analysis most of the sediments can be regarded as mixtures of subglacial and fluvial origins (the samples plot quite distant to the supraglacial control envelope, Figure 26b). The negligible percentage of striations and bullet-shaped clasts, as well as high RA- indices suggests that the samples were unlikely to have been shaped in the subglacial traction zone. However, this evidence does not exclude the subglacial regime as a source of debris provenance. These observations are in contrast with previous case studies in the Himalayas (Scherler et al., 2011; Benn et al., 2012), where the vast majority of samples derives from supraglacial sources. Therefore, it is advisable to further assess the relationship between supraglacial and fluvial process domains (Lukas et al., 2013). In summary, it is apparent that the sediments of *LFA 2* reflect a scattered pattern of distinctive debris pathways (mixed sources: predominantly subglacial, englacial and limited influence of supraglacial sources).

6.1.2 Eastern Lateral Moraine: Lithofacies 3 association 3 (LFA 3)

Lithofacies association 3 differs from the previous lithofacies associations due to the fact that it mostly represents a diamicton with a sandy-gravelly matrix, instead of a fine grained, silty-sandy matrix (being representative of the western lateral moraine). *LFA 3* is interpreted as debris flows that reflect multiple re-advance and retreat events of Suldenferner. Because fine-grained sediments are rare at the eastern lateral moraine, the role of dead-ice incorporation and melt-out is hardly quantifiable (Gribensky et al., 2016 and references therein). But historical observations of ice-marginal oscillations suggest that the lateral moraines did not incorporate dead-ice bodies (ice margin progressively retreating backwards in a linear way). The diamictons contain a huge amount of micaschist clasts which were incorporated into the moraines as extraglacial rockfall (dense jointing/high cleavage of micaschist providing pre-existing planes of weakness for failure). However, the fact that these diamictons also contain clasts of dolomite strongly suggests that at least some of these clasts clasts have been transported purely supraglacially until finally being incorporated into the eastern lateral moraine.

6.1.3 Comparison with Previous Studies on Lateral Moraine Formation in the Alps

The diversity of the study area in the Upper Sulden Valley is ascribed to different reactions to glacial imprint, weathering and erosion of the bedrock. Most of the sedimentary units at Suldenferner are diamictic, stratified, loose and intercalated with sorted sediments. The sediments of both the western and eastern lateral moraine do not contain any evidence of overriding or subglacial shearing. Moreover, already-existing moraines do not show any visual signs of deformation (no trust and fold structures have been detected). This is mainly, because the diamictons that are present within the moraines are friable and poorly consolidated (Reinardy and Lukas, 2009). Further, clast shape analysis reveals that the main mode of sediment delivery cannot be truly subglacial (low degree of subrounded-rounded clasts). In fact, there is an inherent lack of glaciotectonised, pre-existing sediments that have been overconsolidated by multiple glacial advances. The absence of deformational structures is ascribed to an absence of ice-pushing (Benn et al., 2001; Lukas, 2011). This structural evidence is in contrast to previous case studies on clean-ice glaciers in Switzerland (Lukas et al., 2012) and Austria (McMahon, 2015). Further, it has to be considered that the absence of thick, fine-grained units makes the degree of alteration by ice push difficult to quantifiable (Lukas, 2005). The absence of subglacial traction till at Suldenferner is compatible with the sparsity of such sediments at the temperate valley glacier Gornengletscher in Switzerland (Lukas, 2012). Structural evidence of debris-
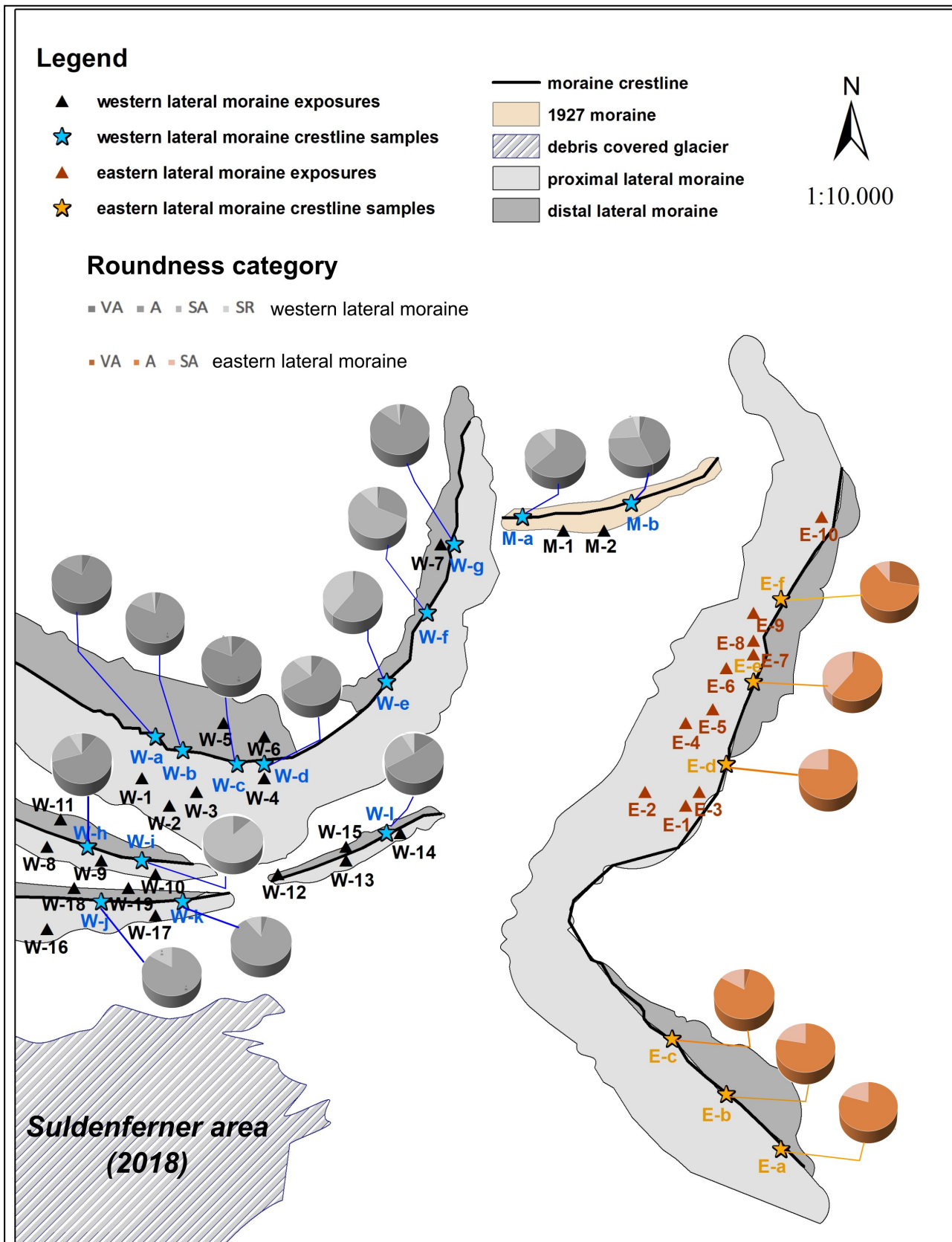
Fig. 24. Overview map of the lateral moraines at Suldenferner, marking the locality of the exposures and the crestline samples. The analysis of clast roundness data is shown of both western (grey pie-charts) and eastern (orange pie-charts) lateral moraines. Note the trend from angular to subangular clasts (western lateral moraine) and the trend from angular to very angular clasts (eastern lateral moraine) with increasing distance to the glacier.
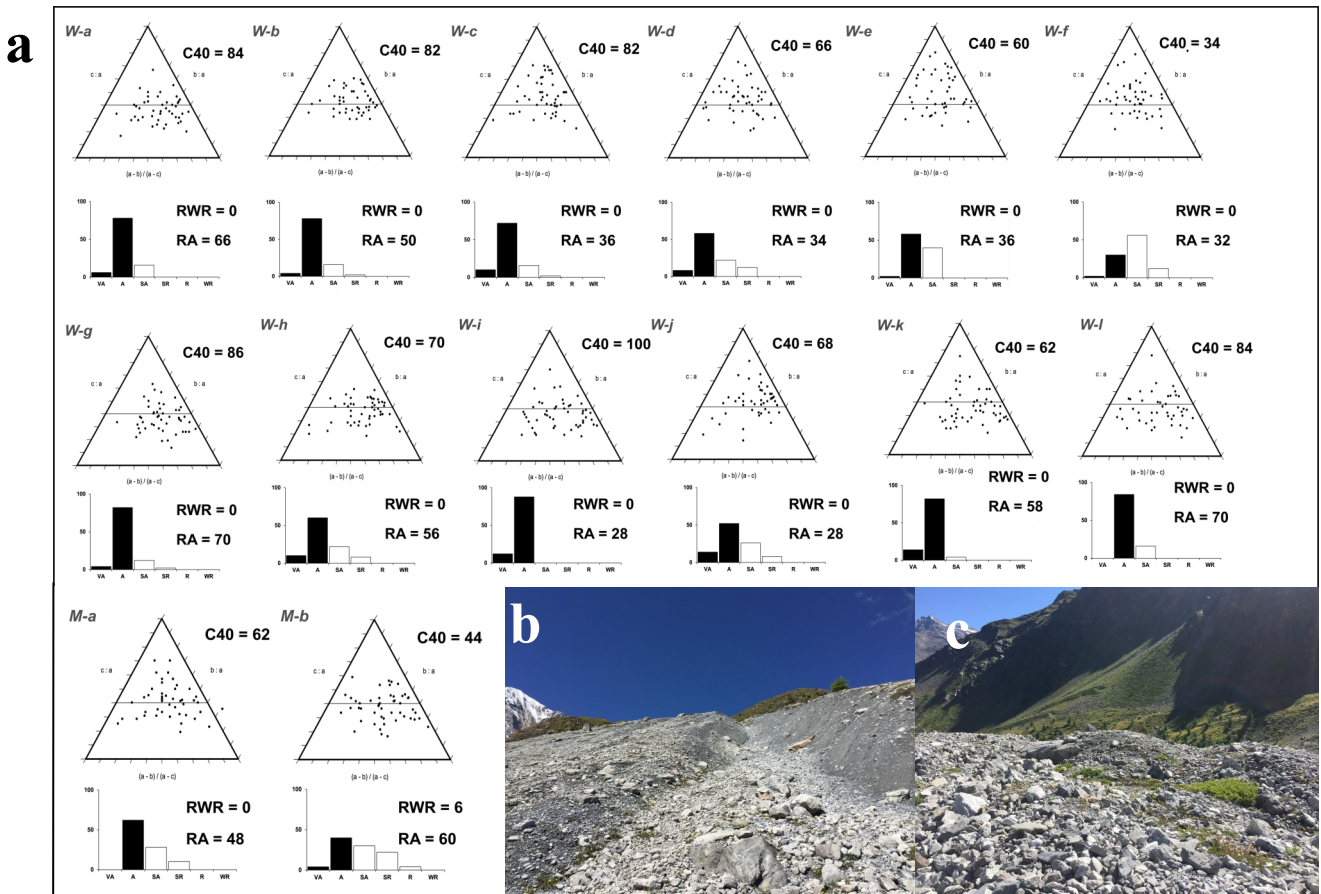
Fig. 25. (a) Ternary diagrams and histograms of the western lateral moraine crestline samples, showing clast form and roundness data, respectively. (b) Debris layers of dolomite on top of the western lateral moraine, view towards E. (c) Accumulation of debris on top of the western lateral moraine, view towards NE.
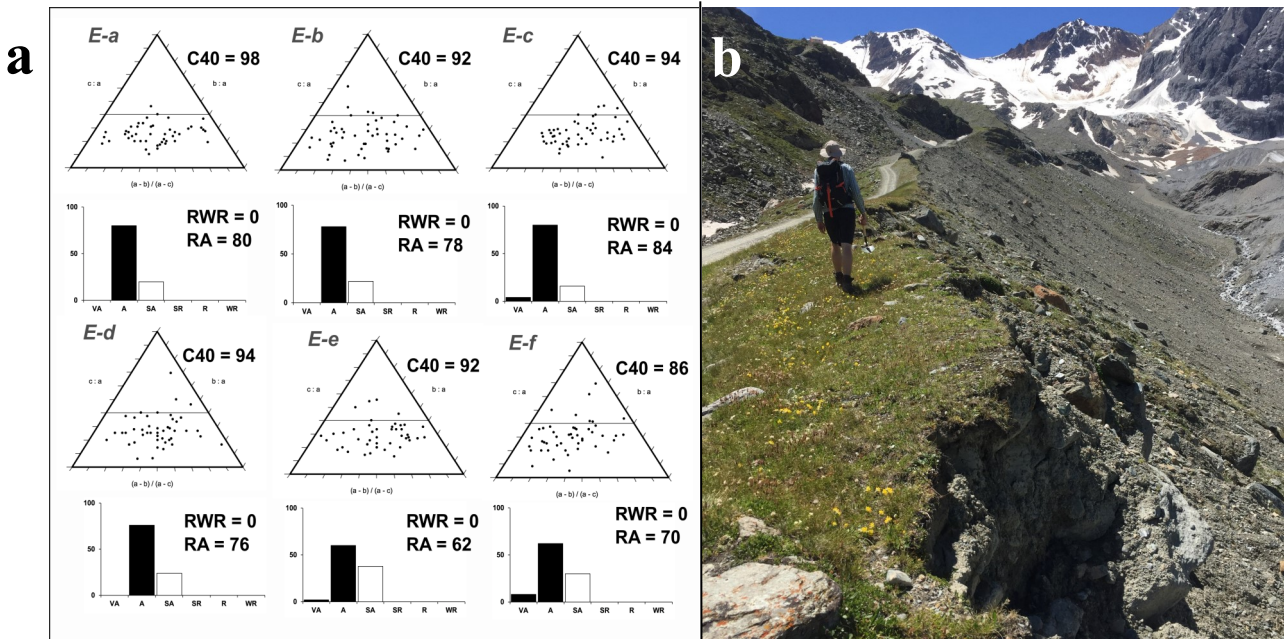

Fig. 26. (a) Ternary diagrams and histograms of the eastern lateral moraine crestline samples, showing clast form and roundness data, respectively. (b) Overview picture of the eastern lateral moraine crestline, view towards S.

dumping and moraine overtopping as important modes of formation are analogous to lateral moraine formation at Schwarzberggletscher (Tonkin, 2016). In the case of Suldenferner the formation of new lateral moraines (lateral accretion after subsequent ice advances (Benn and Evans, 2010) is not traceable. Instead erosional remnants of the western lateral moraine are nowadays detected in the Suldenferner foreland. Renewed debris flow deposition on top of the moraines (Small, 1983) likely took place during subsequent ice advances (i.e. glacial advance during 1817). Due to the fact that the stability of moraines depends on both ice-margin stability and the sediment delivery to the surface (Lukas et al., 2012) it is reasonable to assume that the ice margin was stationary or slowly advancing in the youngest history of Suldenferner (coherent with historical observations, see chapter 3). Dead-ice incorporation and melt-out after withdrawal from ice support play an important role in the foreland of Suldenferner. However, it is doubtful that the lateral moraines have incorporated significant amounts of dead-ice due to a lack of sedimentological evidence and historical observations (cf. Fig. 10f). It is important to consider that extraglacial sources (rockfall) are vital components in ensuring a permanent supraglacial debris cover at Suldenferner. Moreover, fine-grained matrix material within the diamictons was probably generated by glacial crushing and transported via nivation and aeolian processes (Lukas et al. 2005).

It turns out that *LFA 2* is the most frequent lithofacies that has been detected within the western lateral moraine at Suldenferner (66.6%). It is supplemented by *LFA 1* (33.4%). The western lateral moraine was mainly influenced by a low level (active) debris transport through subglacial/englacial and fluvial pathways. This evidence is mainly supported by clast shape analysis (high degree of scattering between the single control envelopes. Supraglacial sources (characterised by high RA-indices, medium C_{40}-indices) also have to be respected, but do not play a such dominant role as observed at debris-covered glaciers in the Himalayas (cf. Scherler et al., 2011). Interestingly, clast shape analysis also reveals that the clasts incorporated into the diamicts are not likely to have been shaped in the subglacial regime (absence of bullet-shaped morphology, lack of striations etc.). This observation is in stark contrast to case studies on clean-ice glaciers in the Alps (Goodsell et al., 2005; Lukas et al., 2012). Because the eastern lateral moraine is more homogeneous in nature as compared to the western lateral moraine, it is standing to reason that only one lithofacies is attributed with the sediments (i.e. *LFA 3*). It turns out that *LFA 1* and *LFA 2* do not vary significantly in character. Indeed, nearly all of the diamictons that have been discovered in the western lateral moraine are friable and easy to excavate, Further,

the diamictons do not show any signs of compaction or cementation. However, some minor differences exist between the lithofacies associations. These differences mostly regard the nature of the sorted sediments and their basal boundaries, as well as the general appearance of the diamictons (see chapter 5.2).

6.2 Clast Shape

The scattered distribution pattern of the samples (Fig. 22, Fig. 23) suggest that the samples are neither truly supraglacial nor fluvial and must display a complex history (potential mix between subglacial, fluvial and englacial sources). It is possible that the formation of the supraglacial debris cover at Suldenferner occurred relatively recently and can be attributed to the melting of the ice surface and a subsequent dispersal of supraglacial debris (Kirkbride and Deline, 2013). This explains the mixed signal of supraglacial, fluvial and potential subglacial control regimes. The initially estimated subglacial control sample is indeed a surface sample in Suldenferners foreland. This assumption is proved by the fact that this sample shows a similar Co-variance plot as the crestline samples of the western lateral moraine (high RA-index being indicative of increased angularity, see Figure 26c). As already demonstrated by Lukas et al. (2013) safety considerations preclude the collection of subglacial control samples in around 50% of the areas from a worldwide selection of glaciated mountain environments. Thus, the lack of true subglacial control samples is a common problem affecting clast shape analyses and not limited to Suldenferner. Overall, the samples of the lateral moraines at Suldenferner are attributable to the Type II catchment (high mountain regions), concerning the debris cascade in glacial environments, because the samples are characterised by a high similarity between subglacial and fluvial control regimes (Lukas et al., 2013).

6.3 Moraine Morphology, Preservation Potential and Stability

While the western lateral moraine at Suldenferner is characterised by nearly uniformly-steep slopes (reaching angles of up to 80°), the eastern lateral moraine is characterised by a stronger cross-profile asymmetry with steeper proximal (40°-60°) and gentler distal (25°-30°) slopes (Fig. 27, Fig. 28). Indeed, it is striking that the proximal slope of the eastern lateral moraine flattens out with increasing distance from the moraine crestline. Contrarily, the western lateral moraine maintains its steep nature from the bottom to the top of the moraine. This exceptional steepness is directly linked to a high stability of the moraines, even though weathering generates distinctive gullies (up to 2 m deep) on both proximal moraine flanks. It is likely

Fig. 27. Close – up photographs of Suldenferner and its foreland. (a) Supraglacial debris cover (view to the southeast). (b) Reworked glaciogenic material (view towards southwest, prominent peak Königsspitze in the background). (c) Densely gullied wall of the eastern lateral moraine. (d) Glacier portal of Suldenferner (view towards east).
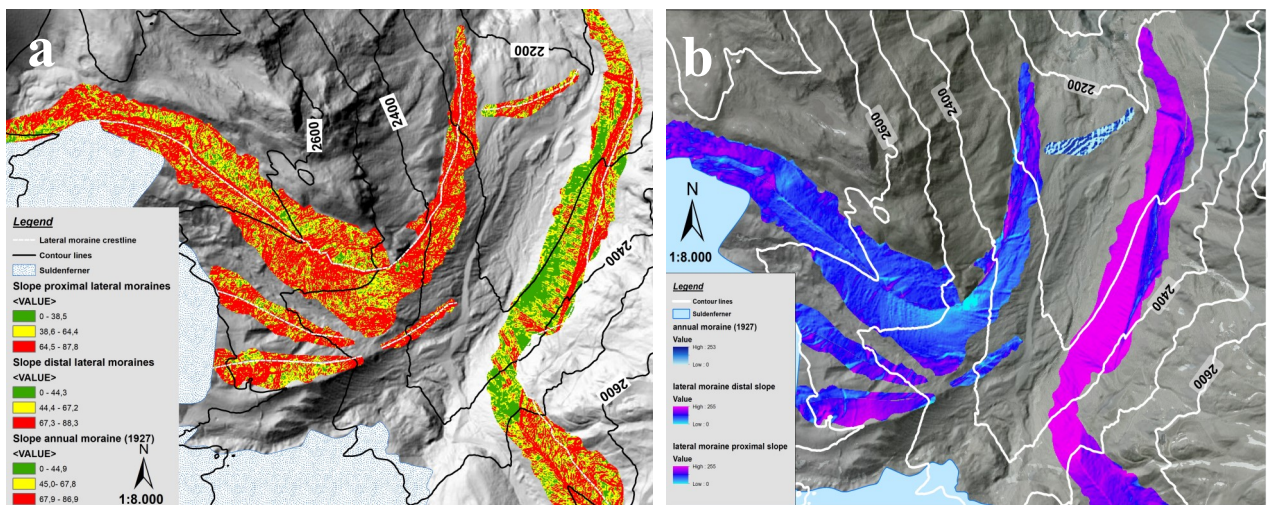

Fig. 28. (a) Slope (°) of the lateral moraines and the 1927 moraine at Suldenferner. (b) Hillshade model of the moraines (supplemented by DTM 2011, Geological Service of South Tyrol, 2018).

37

that the moraines at Suldenferner obtained their stability in the course of paraglacial reworking of the proximal slopes (cf. Curry et al., 2009). Curry et al.'s (2009) observations at Feegletscher (Switzerland) revealed paraglacial processes being responsible for eroding gullies in the upper slope segments of the moraines and associated debris flows being deposited in the mid and slope foot zone at lower angles (between 34° and 25°). This causality is also detectable at the lateral moraines at Suldenferner: sedimentological analysis revealed that cementation and high consolidation are absent in the moraines. The a-axes of most of the clasts were observed to be visually aligned parallel to the distal slopes and appear to confirm Curry et al.s (2009) hypothesis, but clast fabric measurements were not carried out for safety reasons, yet would be required to substantiate this initial observation. Glacial retreat is responsible for dead-ice formation of unknown thickness (Lukas et al., 2012) in the Suldenferner foreland (frontal area of the lateral moraines). The vertical orientations of the clasts in the ice-marginal area highlight the assumption of the presence of dead-ice (Lukas, 2011). This assumption is further aided by the fact that the differential ablation rates at debris–covered glaciers lead to ice preservation (Patterson and Cuffey, 2010; Nicholson and Benn, 2013). In contrast, the sedimentology of the lateral moraines suggests that dead-ice incorporation did not take place into them (no direct evidence of melt-out structures and de-stratification of the units). Moreover, there are only few regimes of sorted sediments in the moraines that could preserve deformational structures. Indeed, the present sediments appear as conformable,, undisturbed, stratified lenses, which precludes the presence of dead-ice (cf. Benn, 1993; Lukas, 2005). This is also coherent with historical observations (see Fig. 10f) as the glacier did not exceed the height of the previously formed lateral moraines. Overall, the exposure conditions in the lateral moraines did not allow for any diagnostic features of dead-ice melt-out to be detected. Densely vegetated areas are frequently present at the distal side of the eastern lateral moraine. Overall, the preservation potential and stability of both the western and eastern lateral moraines is also high, because the moraines are not altered by glaciofluvial reworking (as observed in a case-study on ice-cored moraines with a strong permafrost influence in Svalbard, cf. Lukas et al., 2005).

6.4 Limitations and Suggestions for Future Studies

Even if the lateral moraines at Suldenferner were assessed in detail in terms of sedimentological analysis, a few questions remain unsolved at present and provide scope for future work. These limitations are listed below.

1. Because the role of dead-ice incorporation is still debated it is suggested to monitor the future glacial development at Suldenferner to test whether dead-ice incorporation takes place in the foreland and where in relation to the lateral moraines.

2. Because both lateral moraines at Suldenferner are characterised by steep slopes (reaching angles of up to 80°), exposures could only be dug in restricted parts of the moraines. Therefore, it is recommended to monitor the future development of the moraines with airborne-based, high-resolution LiDAR mapping in order to solve the problems of limited accessibility.

3. Sedimentological analysis revealed a striking similarity between the small moraine dated to 1927 (at the northern rim of the area of former stagnant ice) and the western lateral moraine. Therefore, future studies could address the question of further analysing the sedimentary properties of this small moraine and arriving at a conceptional model of how such smaller moraines form high-alpine settings.

4. Due to the fact, that only a restricted timeframe was scheduled for this master's thesis (as well as a limited budget) GPR measurements (cf. Lukas and Sass, 2011) and seismic analyses were not conducted. However, these methods could add further evidence to add to the present study.

5. Clast fabric analysis (providing evidence of the orientation of the clasts that are incorporated within the exposures) could count as a valuable supplement for lithofacies analysis. Even if the method is time demanding it gives clues about the degree of stress, that the glacier exerted at the adjacent sediments (Hooyer and Iverson, 2000).
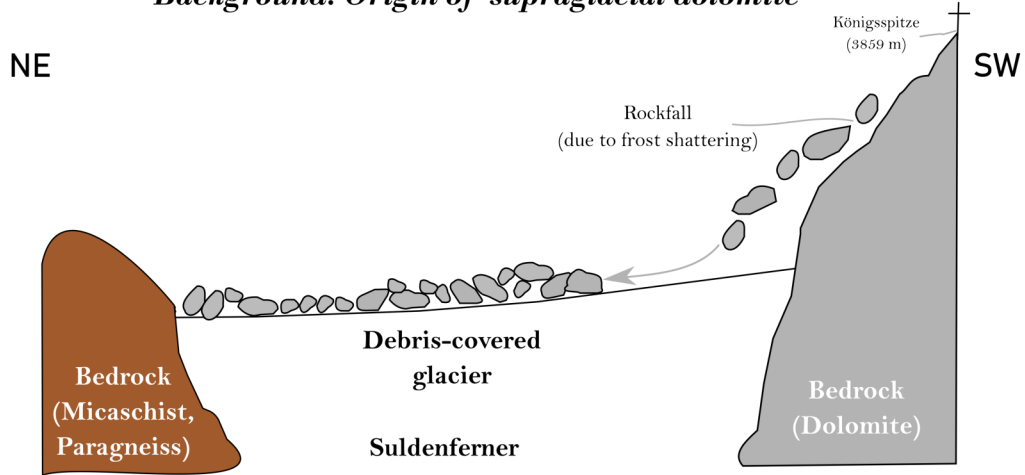
6. It is also interesting to note, that Suldenferner has not always been completely covered with debris. In fact, the glacier was characterised by a partial debris draping (restricted area in the southwest of the glacial body) in the 1980s and an alternating thickness of the debris cover (highest in downglacier areas, Mair, V., pers. comm., 2018). This circumstance likely has influenced the glaciers mass budget (resulting in a differential ablation) and should be taken into account in further investigations and glacial reconstructions.

6.5 Synthesis: Conceptual Model of Lateral Moraine Formation at a Debris-covered Glacier

Both the western and eastern lateral moraines at Suldenferner are extraordinarily well preserved and count as impressive examples of high-alpine lateral moraines. As previously described in the literature (Benn et al., 2003; Lukas et al., 2012; McMahon 2015) the genesis of the moraines can be inserted into the concept of the glaciated valley landsystem (Boulton and Eyles, 1979). The evidence presented below specifically concerns the development of debris-covered glaciers in Alpine settings and respects variations that

Background: Origin of supraglacial dolomite

NE

SW

Königsspitze
(3859 m)

Rockfall
(due to frost shattering)

Debris-covered
glacier

Suldenferner

Bedrock
(Micaschist,
Paragneiss)

Bedrock
(Dolomite)

A) Initial phase of lateral moraine formation

NW

SE

Debris-flow dominated
ice-contact fan
(mixed sources: supraglacial,
subglacial and
englacial sources)

Melt-out of
englacial sediment

Debris-flow dominated ice-contact fan
(supraglacial and
extraglacial sources)

Rockfall: gravitational
sliding
along shear planes

Debris-covered
glacier

Suldenferner

Englacial debris septa

Englacial debris septa

Subglacial
meltwater
channels

Bedrock
(Micaschist,
Paragneiss)

Bedrock
(Micaschist,
Paragneiss)

B) Initital phase of glacier retreat

NW

SE

Collapse of proximal sediments;
ice-contact face formation

Collapse of proximal sediments;
ice-contact face formation

Openwork gravel
accumulation

Debris-covered
glacier

Suldenferner

Englacial debris septa

Englacial debris septa

Subglacial
meltwater
channels

Bedrock
(Micaschist,
Paragneiss)

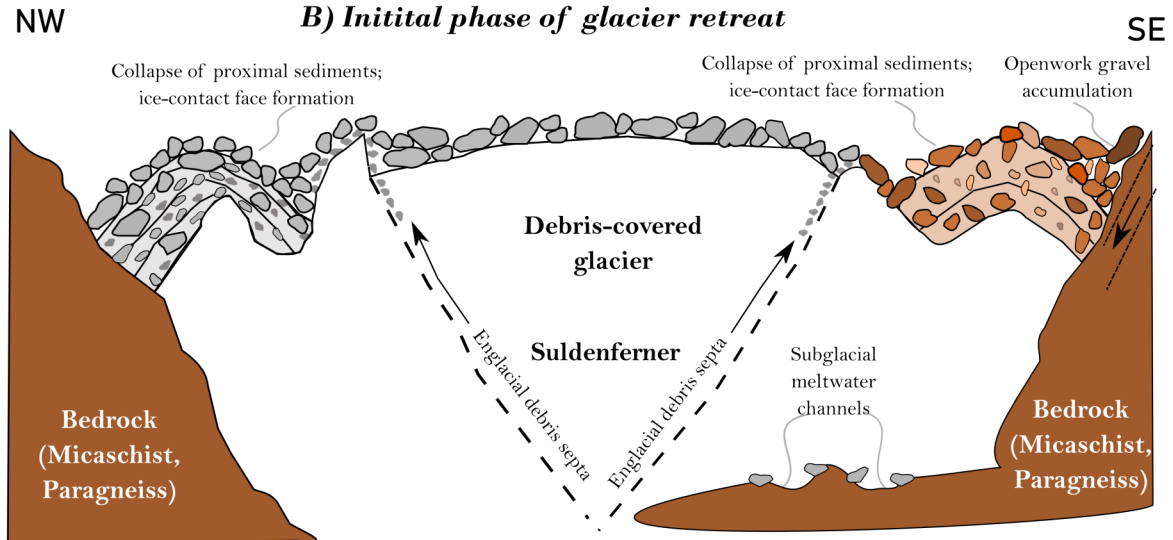Bedrock
(Micaschist,
Paragneiss)

Fig. 29. Schematic diagram representing the conceptual model of the western lateral moraine formation at Suldenferner. This process model is based on both sedimentological analysis and comparison with previous studies (Lukas et al., 2012; McMahon, 2015).
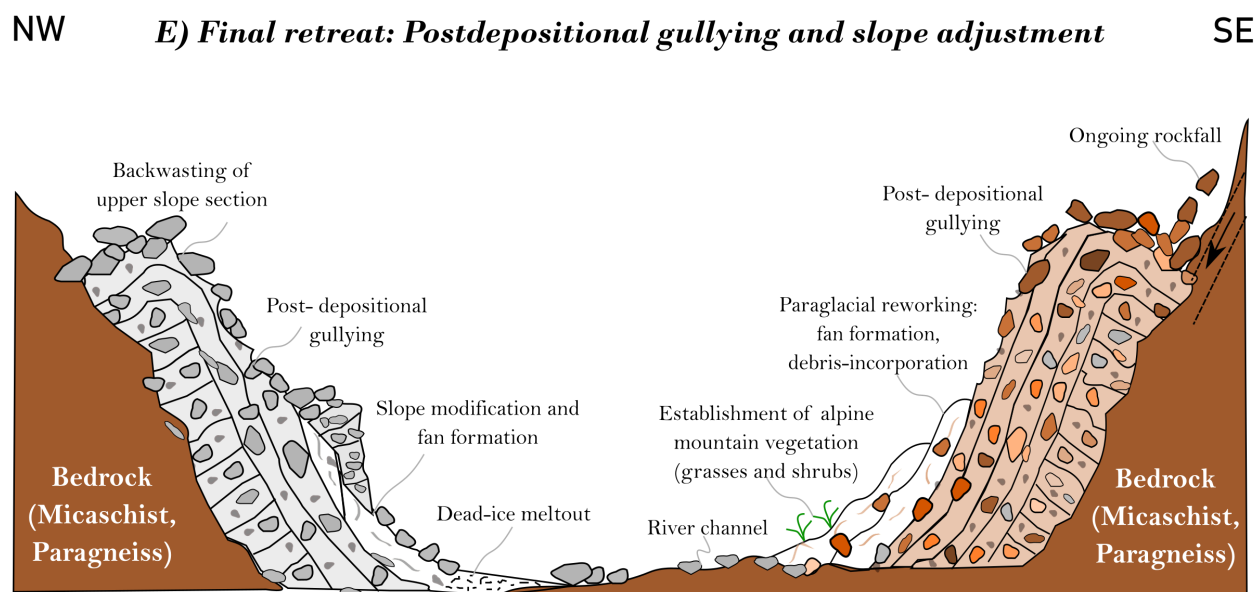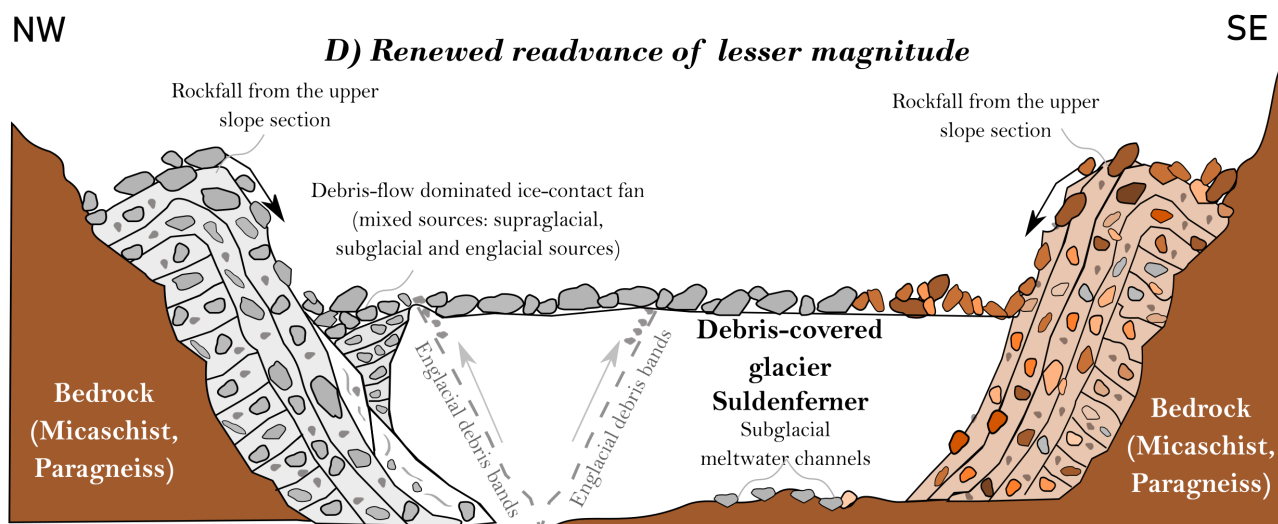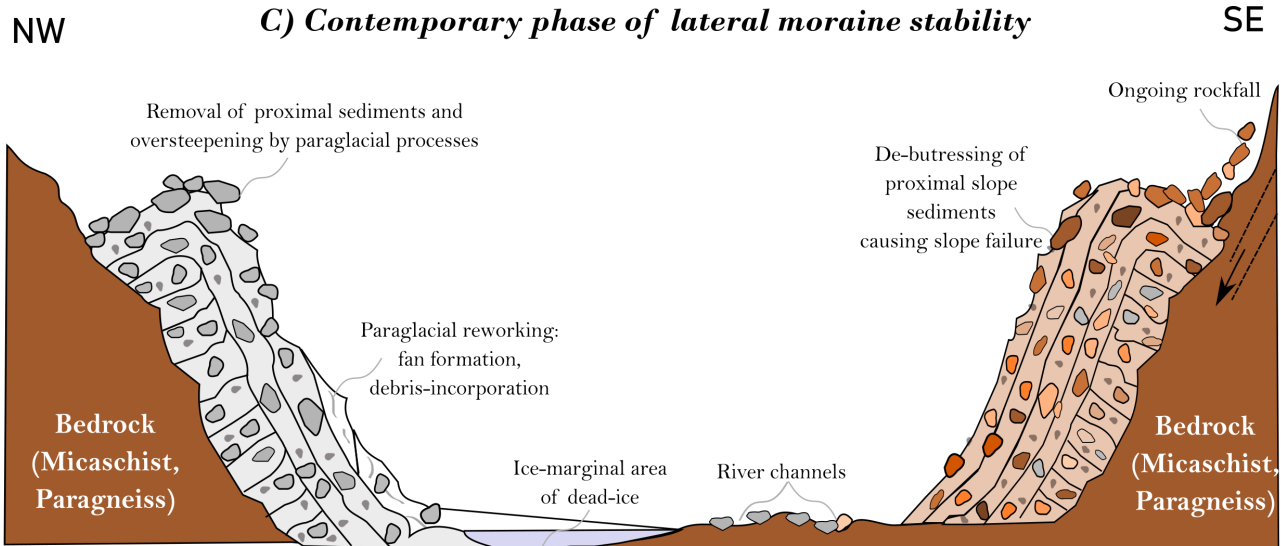
C) Contemporary phase of lateral moraine stability

NW

SE

Removal of proximal sediments and
oversteepening by paraglacial processes

Ongoing rockfall

De-butressing of
proximal slope
sediments
causing slope failure

Paraglacial reworking:
fan formation,
debris-incorporation

**Bedrock
(Micaschist,
Paragneiss)**

Ice-marginal area
of dead-ice

River channels

**Bedrock
(Micaschist,
Paragneiss)**

NW

SE

D) Renewed readvance of lesser magnitude

Rockfall from the upper
slope section

Rockfall from the upper
slope section

Debris-flow dominated ice-contact fan
(mixed sources: supraglacial,
subglacial and englacial sources)

**Bedrock
(Micaschist,
Paragneiss)**

Englacial debris bands

Englacial debris bands

**Debris-covered
glacier
Suldenferner**
Subglacial
meltwater channels

**Bedrock
(Micaschist,
Paragneiss)**

NW

E) Final retreat: Postdepositional gullying and slope adjustment

SE

Backwasting of
upper slope section

Ongoing rockfall

Post- depositional
gullying

Post- depositional
gullying

Paraglacial reworking:
fan formation,
debris-incorporation

Slope modification and
fan formation

Establishment of alpine
mountain vegetation
(grasses and shrubs)

**Bedrock
(Micaschist,
Paragneiss)**

Dead-ice meltout

River channel

**Bedrock
(Micaschist,
Paragneiss)**

Fig. 29. Continued.

40

may be encountered in different localities.

Suldenferner's supraglacial debris cover mainly consists of dolomite clasts. These clasts originate from the steep walls of the Königsspitze (southwestern bedrock catchment) that frequently experience rockfall due to frost-shattering (top panel in Fig. 29). Dolomite clasts are also transported via avalanches across steep icefalls (specifically during the ablation season). Another mode of dolomite transport is ascribed to subglacial clast components that are transported to the glacier surface across englacial debris septa. In fact, these dolomite clasts accumulate on top of the glacier and are transported to the glacial snout via gravitational flow processes. This results in an increased debris thickness (between 40 and 67 cm) at the glacier terminus (L.I. Nicholson, pers. comm., 2018).

Sedimentological investigations and clasts shape measurements reveal that glacial sediment at Suldenferner derives from mixed sources. The western lateral moraine is most significantly influenced by the following derivations: (i) from the aforementioned rockfall from the Königsspitze (angular clasts, extraglacial/supraglacial origin) and (ii) subrounded-subangular clasts (subglacial origin) that are elevated along englacial shear planes (Figure 30a). Processes of freeze- on and progressive melt-out of sediment on the surface follow the aforementioned glacial development. Currently, the eastern lateral moraine is mainly influenced by three sources: (i) extraglacial clasts originating from rockfall (mainly micaschist from the eastern bedrock catchment), (ii) subglacial dolomite clasts that are transported via englacial debris septa and (iii) supraglacial dolomite components. These processes of debris delivery take place during glacial advance. At the same time, subglacial meltwater channels transport meltwater and clasts downvalley.

Debris-flow dominated, ice-contact fans of supraglacial, fluvial and englacial/subglacial sources mark the primary stage of western lateral moraine genesis. This structural evidence is derived from co-variance analysis (Fig. 22). However, it has to be stated that fluvial, subglacial and supraglacial sources are not clearly distinguishable from each other as observed in lateral moraine investigations on Alpine clean ice-glaciers (e.g. Lukas et al., 2012). The control envelopes rather overlap and highlight the fact that the glacier is influenced by a signal of mixed sources. However a subglacial shaping of the clasts can be excluded, because no direct thrust, shear and fold structures were detected during sedimentological analysis (see chapter 5.2). Ongoing rockfall is observable in the form of gravitational sliding across shear planes, depositing additional debris material (micaschist and paragneiss) on top of the ice-contact fan at the eastern lateral moraine.

The initial phase of glacial retreat is marked by a collapse of proximal sediments, resulting in an ice-contact face formation at both the western and eastern lateral moraines (Fig. 29b). The top of the eastern lateral moraine is characterised by an accumulation of openwork gravel (mainly micaschist and paragneiss), whereas the top of the western lateral moraine is exclusively draped by clasts of dolomite.

After a first stage of complete deglaciation the top of western lateral moraine is remarkably over-steepened by paraglacial processes (Fig. 29c). Transiently, the proximal sediments of the eastern lateral moraine are altered by de-buttressing and cause slope failure. During the ablation season the moraines' matrix becomes water-saturated, subsequently mobilised and proceeding down-valley as debris-flows. Progressively, these flows slow down until finally becoming stationary and creating ice-contact fans (emerging as parallel ramps to the ice margin). The amount of ramp deposition vitally relies on the degree of debris delivery from the surface and the time of ice margin stability (Lukas et al., 2012). Moreover, the lower proximal flank of the western lateral moraine experience paraglacial reworking in the form of fan formation and enhanced debris incorporation (mainly dolomite). An ice-marginal area of dead-ice is preserved on the valley bottom, adjacent to the western lateral moraine. This structural evidence is derived from sedimentological investigations in the Suldenferner foreland (see chapter 6). The temporary retreat of Suldenferner causes former subglacial meltwater channels to turn into river channels. This results in a increased roundness of dolomite clasts (higher RWR-indices, see chapter 5.3).

A renewed glacial re-advance of lesser magnitude is followed by the formation of an additional debris-flow dominated, ice-contact fan (mixed sources: supraglacial, subglacial and englacial derivations). This fan is progressively stacked on the main corpus of the western lateral moraine, resembling a small, inset lateral moraine (Fig. 29d). This smaller lateral moraine is likely to follow a similar mode of generation as the lateral moraines assessed at Waxeggkees (see McMahon, 2015 for a review). It is draped by dolomite boulders that originate from the upper slope section. Further, minor glacial advances are believed to deposit young minor moraines at the margins of the western lateral moraine. This is hypothesis is based on the presence of small, 10-20 m wide moraine ridges that emerge parallel to the western lateral moraine. Lateral plastering of reworked pre-existing sediment which originates from slumping and debris cones also took place (hard, consolidated sediment drapes had to be scraped to get close to the in-situ sediment). However, the sediments are not influenced by the appearance of a subglacial traction till due to a lack of overconsolidation (friable nature of sampled diamictons). Transiently, the glacial surface is draped by clasts of micaschist and paragneiss in the southeast (originating from the upper slope section of the eastern lateral moraine). A

final glacial retreat favours the backwasting of the upper slope sections and post-depositional gullying of the moraines (Fig. 29e). These processes create an undulating surface of the lateral moraine flanks. Final slope modification and fan formation (decreasing flow velocity of gravity flows) of the lower parts of the western lateral moraine occur during dead-ice melt-out in the foreland (frontal area) of Suldenferner. Paraglacial processes result in a removal of proximal sediments and cause an oversteepening of the flank. The fans at the bottom of the eastern lateral moraine are finally colonised by alpine mountain vegetation (mainly grasses and shrubs). This last stage of fan formation (dynamics of paraglacial processes) is currently observable at the western lateral moraine of Suldenferner. The conceptual model presented above corresponds well to the previous work Lukas et al. (2012), McMahon (2015) and Tonkin (2016).

7 Conclusions

Evidence of geomorphological mapping and sedimentological analysis has been used to develop a conceptional model of lateral moraine formation at the debris-covered glacier Suldenferner (Vedretta di Solda) in the Eastern European Alps. In order to put the results into a broader perspective a comparison with pre-existing case studies (Lukas et al., 2012; McMahon, 2015; Tonkin, 2016) has been conducted. Finally, the following conclusions can be drawn:

1. Geomorphological mapping of the Suldenferner foreland has revealed the primary elements of the high-alpine glacial environment: (i) the western and eastern lateral moraines, (ii) areas of stagnant ice, (iii) a moraine from 1927, (iv) ice-moulded bedrock giving the direction of ice-flow, (v) outwash terraces, (vi) erosional remnants of the lateral moraines, (vii) gullied glaciogenic material and (vii) glacially-overridden outwash.

2. Both lateral moraines at Suldenferner are up to 130 m high and 3 km long. The main planform of the western lateral moraine is asymmetric, with steep slopes reaching up to 80°. The eastern lateral moraine is characterised by a stronger cross profile asymmetry, with gentle distal (25°-30°) slopes and steeper proximal (40–60°) slopes. The proximal slopes of both the western and eastern lateral moraine are intensively gullied. However, the most distinctive differences between the moraines comprise their shape/ distribution and sedimentary composition. The western lateral moraine is accompanied by a set of subsidiary branches (up to 500 m in length) and does not show any signs of vegetation in contrast to the eastern lateral moraine. Moreover, the lithology of clasts incorporated within the western lateral moraine comprises exclusively clasts of dolomite, whereas the eastern lateral moraine contains boulders of micaschist, some

dolomite and paragneiss.

3. Sedimentological analysis allows insights into the mechanisms of lateral moraine formation in high-alpine settings. Two lithofacies associations (*LFA 1, LFA 2*) are distinguished for the western lateral moraine, and *lithofacies association 3 (LFA 3)* is found at the eastern lateral moraine. *LFA 1* primarily consists of a silty-sandy, friable, graded, matrix-supported diamicton ($DgMm_1$-2) and intercalated lenses of sorted sediments. This lithofacies association is variable distributed across the main branch of the western lateral moraine and interpreted as reworked glaciofluvial deposits that accumulate between the proximal flank of the moraine and the glacier. *LFA 2* consists of a fine-grained, clast-rich, matrix-supported, clayey-silty diamicton ($DgFm_2$-2) and a clayey-silty, massive diamicton ($DhMm_3$-2). Being the most frequent lithofacies association at Suldenferner it is interpreted as supraglacial debris flows that have been deposited from a subaerial position. Some of the massive, homogeneous, matrix-supported, friable, fine-grained, clayey-silty diamictions ($DhMm_3$-2) contained within *LFA 2* are interpreted as stacked, coalesced, ice-contact debris fans. *LFA 3* is built up of a massive, homogeneous coarse-grained (sandy-gravelly) diamicton ($DmCm_1$-1). The diamicton is matrix- supported and loose (not compacted) and interpreted as subaerial debris flows that incorporate distinctive amounts of extraglacial rockfall.

4. Clast shape results reveal a scattered pattern of distinctive debris pathways. Material preserved within the moraines results from a mix of primarily subglacial/ englacial sources and supplemented with debris from fluvial, supraglacial and extraglacial origin. It turns out that glaciofluvial debris is elevated to an ice-marginal (supraglacial) position by freeze-on of englacial debris bands. Interestingly, there is no direct evidence for a subglacial shaping of the clasts as reported on previous studies that focused on clean-ice glaciers in the Alps (Lukas and Sass, 2011, Lukas et al., 2012). This is mainly because the sediments are not compacted or cemented and that there is in inherent lack of bullet-shaped and striated clasts, as well as an absence of subglacial traction tills. Therefore, it is legitimate to assume that the main sediment delivery of a debris-covered glacier is a mixed signal of subglacial, englacial, fluvial and supraglacial derivations. Overall, the results contradict a predominant supraglacially input of debris as estimated in previous case studies on debris-covered glaciers in the Himalayas (Scherler et al., 2011). Further, clast shape analysis indicates that the climate signal of debris-glaciers in high-alpine settings is more nuanced, excluding a predominant subglacial component (as clean-ice glaciers contain, Lukas et al., 2012) and demonstrating the presence of multiple "mixed" process domains, covering a wide spectrum ranging between fluvial, subgla-

cial and supraglacial derivations.

8 Acknowledgements

9 References

Aber, J. S. and Krüger, J. (1999).” Formation of supraglacial sediment accumulations on Kötlujökull, Iceland.” Journal of Glaciology, **45** (150): 400-402.

Benn, D.I., and Ballantyne C.K. (1993). “The description and representation of particle shape.” Earth Surface Processes and Landforms, **18**: 665-672.

Benn, D.I., and Ballantyne C.K., (1994). “Reconstructing the transport history of glacigenic sediments: a new approach based on the co-variance of clast shape indices.” Sedimentary Geology, **91**: 215-227.

Benn, D.I., Kirkbride, M.P., Owen, L.A., Brazier, V. (2003). “Glaciated valley landsystems.” In: Evans, D.J.A. (Ed.), Glacial Landsystems. Ar-

nold, London: 372-406.

Benn, D.I., and Evans, D.J.A., (2010). “Glaciers and Glaciation, second ed.” Arnold, London, 802 pp.

Benn, D.I., Bolch, T., Hands, K., Gulley, J. Luckman, A., Nicholson, L.I., Quincey, D., Thompson, S., Toumi, R., Wiseman, S. (2012). "Response of debris-covered glaciers in the Mount Everest region to recent warming, and implications for outburst flood hazards." Earth-science reviews, **114**(1-2): 156-174.

Boulton, G.S., and Eyles, N. (1979). “Sedimentation by valley glaciers; a model and genetic classification.” In: Schlüchter, C. (Ed.), Moraines and Varves. Balkema, Rotterdam: 11-23.

Brock, B.W., Mihalcea, C., Kirkbride, M.P., Dioaiuti, G., Cutler, M.C., Smiraglia, C. (2010).“Meteorology and surface energy fluxes in the 2005-2007 ablation seasons at the Miage debris-covered glacier, Mont Blanc Massif, Italian Alps.“ Journal of geophysical research: atmospheres, **115** (D9).

Brook, M. S., and Lukas S. (2012). "A revised approach to discriminating sediment transport histories in glacigenic sediments in a temperate alpine environment: a case study from Fox Glacier, New Zealand." Earth Surface Processes and Landforms, **37**(8): 895-900.

Carturan, L., Filippi, R., Seppi, R., Gabrielli, P., Notarincola, C., Bertoldi, L., Paul, F., Rastner, P., Cazorzi, F., Dinale, R., Dalla Fontana, G. (2013). "Area and volume loss of the glaciers in the Ortles-Cevedale group (Eastern Italian Alps): controls and imbalance of the remaining glaciers." The Cryosphere, **7**(5): 1339-1359.

Chandler, B. M., Lovell, H., Boston, C. M., Lukas, S., Barr, I. D., Benediktsson, Í. Ö., Ewertowski, M.W. (2018)."Glacial geomorphological mapping. A review of approaches and frameworks for best practice." Earth-science reviews, **185**: 806-846.

Citterio, M. Diolaiuti, G., Smiraglia, C., D´agata, C., Carnielli, T., Stella, G., Siletto, G.B. (2007).” The fluctuations of Italian glaciers during the last century: a contribution to knowledge about Alpine glacier changes.” Geogr. Ann., **89**:164–182.

Curry, A., Sands, T.B., Porter, P.R. (2009). “Geotechnical controls on a steep lateral moraine undergoing paraglacial slope adjustment.” In: Knight, J., Harrison, S. (Eds.), Periglacial and Paraglacial Processes and Environments. The Geological Society, London, Special Publications: 181-197.

Collier, E., Maussion, F., Nicholson, L.I., Mölgg, T., Immerzeel, W.W., Bush, A.B.G. (2015). "Impact of debris cover on glacier ablation and atmosphere-glacier feedbacks in the Karakoram." Cryosphere, **9**(4): 1617-1632.

Desio, A. (1967). "I Ghiacciai del Gruppo Ortles-Cevedale (Alpi Centrale)"- Torino.

Dutto, F., and Mortara, G. (1992). "Glacial hazards in the Italian Alps." ISN 0391-9838.

Evans, D. J. A., and Benn, D. I. (2004)." A Practical Guide to the Study of Glacial Sediments." Arnold, London:78-92.

Finsterwalder, S. (1887). "Der suldenferner." Zeitschrift des Deutschen und Osterreichischen Alpenvereins, **18**: 72-89.

Goodsell, B., Hambrey, M. J., Glasser, N.F. (2005). "Debris transport in a temperate valley glacier: Haut Glacier d´Arolla, Valais, Switzerland." Journal of Glaciology, **51** (172): 139-146.

Graham, D. J. and N. G. Midgley (2000). "Graphical representation of particle shape using triangular diagrams: an Excel spreadsheet method." Earth Surface Processes and Landforms, **25** (13): 1473-1477.

Gribenski, N., Jansson, K.N., Lukas, S., Stroeven, A.P., Harbor, J.M., Blomdin, R., Clifton, T. (2016). "Complex patterns of glacial advances during the late glacial in the Chagan Uzun Valley, Russian Altai." Quaternary Science Reviews, 149: 288-305.

Haidong, H., Yongjing, D., Shiyin, L. (2006). "A simple model to estimate ice ablation under a thick debris layer." Journal of Glaciology, **52**(179): 528-536.

Hambrey, M. J., Christoffersen, P., Glaser, N. F., Hubbard, B. (2009)."Glacial sedimentary processes and products". John Wiley & Sons, Vol. 23.

Hooyer, T.S. and Iverson, N.R. (2000). "Clast fabric development in a shearing, granular material: Implications for subglacial till and fault gauge."GSA Bulletin, **112** (5): 683-692.

Keim, L., Mair, V., Morelli, C. (2017)."General Geologic map of South Tyrol." Published and unpublished results of the CARG and Basiskarte projects, the Italian geological map 1.100,000, and the Structural model of Italy 1:500,000 (ed. 1990).

Kellerer-Pirklbauer, A., Lieb G.K., Avian, M., Gspurnig J. (2008)."The response of partially-debris-covered valley glaciers to climate change: the example of the Pasterze Glacier (Austria) in the period 1964 to 2006." Geografiska annaler: Series A, Physical Geography, **90**(4): 269-285.

Kirkbride, M. P., and A. J. Dugmore (2003). "Glaciological response to distal tephra fallout from the 1947 eruption of Hekla, south Iceland." Journal of Glaciology, **49**(166): 420-428.

Kirkbride, M.P., and Deline, P. (2013)"The formation of supraglacial debris covers by primary dispersal from transverse englacial debris bands." Earth Surface Processes and Landforms, **38** (15): 1779-1792.

Knoll, C., and H. Kerschner (2009). "A glacier inventory for South Tyrol, Italy, based on airborne laser-scanner data." Annals of Glaciology, **50** (53): 46-52.

Krüger J., and Kjaer K. H. (1999)"A data chart for field description and genetic interpretation of glacial diamicts and associated sediments...with examples from Greenland, Iceland and Denmark." Boreas, **28** (3): 386-402.

Lukas, S. (2005). "A test of the englacial thrusting hypothesis of `hummocky` moraine formation: case studies from the northwest Highlands, Scotland." Boreas, **34** (3): 287-307.

Lukas, S., Nicholson, L.I., Ross, F.H., Humlum, O. (2005). "Formation, meltout processes and landscape alteration of high-arctic ice-cored moraines - examples from Nordenskiöld Land, central Spitsbergen." Polar Geography, 29: 157-187.

Lukas, S., and Sass, O. (2011). "The Formation of Alpine Lateral Moraines Inferred from Sedimentology and Radar Reflection Patterns. A Case Study from Gornergletscher, Switzerland." In: Geological Society of London Special Publications, 354:77-92.

Lukas, S. (2011). "Ice-cored moraines."Encyclopedia of Ice, Snow and Glaciers: 616-619.

Lukas, S. (2012). "Processes of annual moraine formation at a temperate alpine valley glacier: insights into glacier dynamics and climatic controls." Boreas, **41**(3): 463-480.

Lukas, S., Graf, A., Coray, S., Schlüchter, C. (2012). "Genesis, stability and preservation potential of large lateral moraines of Alpine valley glaciers–towards a unifying theory based on Findelengletscher, Switzerland." Quaternary Science Reviews, **38**: 27-48.

Lukas, S., Benn, D.I., Boston, C.M., Brook, M., Coray, S., Evans, D.J.A, Graf, A., Kellerer-Pirklbauer A., Kirkbride, M.P., Krabbendam, M., Lovell, H., Machiedo, M., Mills, S.C., Nye, K., Reinardy, B.T.I, Ross, F.H., Signer,

M. (2013). "Clast shape analysis and clast transport paths in glacial environments: A critical review of methods and the role of lithology." Earth-science reviews, **121**: 96-116.

Mair, V. and Stingl, V. (2014). "Einführung in die Geologie Südtirols (Bozen)." Autonome Provinz Bozen.

McMahon, H. (2015). "A contemporary example of lateral moraine formation at Waxeggkees, Austria, utilising geomorphological mapping and sedimentological analysis." Independent Geographical Study, Department of Geography and Environmental Science, Queen Mary University of London, Unpublished BSc thesis, 57 p.

McMahon, H. (2016). "Mechanisms of high-Alpine lateral moraines and implications for glacier dynamics and landscape formation." Department of Geography and Environmental Science, Queen Mary University of London, Unpublished MSc thesis.

Montrasio, A., Berra, F., Cariboni, M., Ceriani, M., Deichmann N., Ferliga C., Gregnanin, A., Guerra, S., Guglielmin, M., Jadoul, F., Longhin, M., Mair, V., Mazzoccola, D., Sciesa, E., Zappone, A. (2012): "Carta Geologica d´Italia, alla Scala di 1:50,000; Foglio 024, Bormio."

Nagai, H., Fujita, K., Nuimura, T., Sakai, A. (2013). "Southwest-facing slopes control the formation of debris-covered glaciers in the Bhutan Himalaya." The Cryosphere, **7** (4): 1303-1314.

Nakawo, M., and Young, G.J. (1981)."Field experiments to determine the effect of a debris layer on ablation of glacier ice." Annals of Glaciology, **2**: 85-91.

Nicholson, L.I. and Benn, D.I. (2013). "Properties of natural supraglacial debris in relation to modelling sub-debris ice ablation." Earth Surface Processes and Landforms **38**(5): 490-501.

Nicholson, L. (2015)."The extent of Suldenferner glacier."News&Blog, www.lindsey.nicholson.org, retrieval: Janurary, 2, 2019.

Nicolussi K., and Stötter H. (1995). „Zur Geschichte der Gletscher der nördlichen Ortlergruppe im 19. und 20. Jh." Department of Geography, University of Innsbruck, Austria.

Patterson, W., and Cuffey, K. (2010). "The Physics of Glaciers". Vol. 2, Elsevier, Amsterdam.

Popovnin, V. V., and Rozova, A. V. (2002). "Influence of Sub-Debris Thawing on Ablation and Runoff of the Djankuat Glacier in the Caucasus:

Selected paper from EGS General Assembly, Nice, April-2000 (Symposium OA36)." Hydrology Research, **33**(1): 75-94.

Reinardy, B., and Lukas, S. (2009)." The sedimentary signature of ice-contact sedimentation and deformation at macro-and micro-scale: A case study from NW Scotland." Sedimentary Geology, **221** (1-4): 87-98.

Reynolds, J. M. (2000). "On the formation of supraglacial lakes on debris-covered glaciers." IAHS publication: 153-164.

Scherler, D., Bookhagen, B., Strecker, M.R. (2011). "Spatially variable response of Himalayan glaciers to climate change affected by debris cover." Nature Geoscience, **4**(3): 156.

Shroder, J. F, Bishop, M.P., Copland, L., Sloan, V.F. (2000)."Debris-covered glaciers and rock glaciers in the Nanga Parbat Himalaya, Pakistan."Geografiska annaler, Physical Geography, **82** (1): 17-31.

Small, R. J. (1983)."Lateral moraines of Glacier de Tsifdjiore Nouve: form, development and implications." Journal of Glaciology, **29** (102): 250-259.

Sneed, E. D., and Folk, R.L. (1978). "Pebbles in the lower Colorado River, Texas a study in particle morphogenesis." The Journal of Geology **66**(2): 114-150.

Spedding, N. and Evans, D.J.A. (2002)."Sediments and landforms at Kvíárjökull, southeast Iceland: A reappraisal of the glaciated valley landsystem." Sedimentary Geology, **149**(1): 21-42.

Stötter, J., Fuchs, S., Keiler, M., Zischg, A. (2003). "Oberes Suldental. Eine Hochgebirgsregion im Zeichen des Klimawandels." Geographischer Exkursionsführer Europaregion Tirol, Südtirol, Trentino. Spezialexkursionen in Südtirol, Innsbrucker Geographische Studien: 33-36.

Tonkin, T.N. (2016). "Characteristics of lateral-frontal moraine formed at Arctic and Alpine glaciers." Nothingham Trent University, Doctoral Dissertation.

Vere, D.M., and Benn, D.I. (1989)."Structure and debris characteristics of medial moraines in Jotunheimen, Norway: implications for moraine classification." Journal of Glaciology, **35**(120): 276-280.

**Tidigare skrifter i serien
"Examensarbeten i Geologi vid Lunds universitet":**

500. Goodship, Alastair, 2017: Dynamics of a retreating ice sheet: A LiDAR study in Värmland, SW Sweden. (45 hp)
501. Lindvall, Alma, 2017: Hur snabbt påverkas och nollställs luminiscenssignaler under naturliga ljusförhållanden? (15 hp)
502. Sköld, Carl, 2017: Analys av stabila isotoper med beräkning av blandningsförhållande i ett grundvattenmagasin i Älvkarleby-Skutskär. (15 hp)
503. Sällström, Oskar, 2017: Tolkning av geofysiska mätningar i hammarborrhål på södra Gotland. (15 hp)
504. Ahrenstedt, Viktor, 2017: Depositional history of the Neoproterozoic Visingsö Group, south-central Sweden. (15 hp)
505. Schou, Dagmar Juul, 2017: Geometry and faulting history of the Long Spur fault zone, Castle Hill Basin, New Zealand. (15 hp)
506. Andersson, Setina, 2017: Skalbärande marina organismer och petrografi av tidigcampanska sediment i Kristianstadsbassängen – implikationer på paleomiljö. (15 hp)
507. Kempengren, Henrik, 2017: Föroreningsspridning från kustnära deponi: Applicering av Landsim 2.5 för modellering av lakvattentransport till Östersjön. (15 hp)
508. Ekborg, Charlotte, 2017: En studie på samband mellan jordmekaniska egenskaper och hydrodynamiska processer när erosion påverkar släntstabiliteten vid ökad nederbörd. (15 hp)
509. Silvén, Björn, 2017: LiDARstudie av glaciala landformer sydväst om Söderåsen, Skåne, Sverige. (15 hp)
510. Rönning, Lydia, 2017: Ceratopsida dinosauriers migrationsmönster under krittiden baserat på paleobiogeografi och fylogeni. (15 hp)
511. Engleson, Kristina, 2017: Miljökonsekvensbeskrivning Revinge brunnsfält. (15 hp)
512. Ingered, Mimmi, 2017: U-Pb datering av zirkon från migmatitisk gnejs i Delsjöområdet, Idefjordenterrängen. (15 hp)
513. Kervall, Hanna, 2017: EGS - framtidens geotermiska system. (15 hp)
514. Walheim, Karin, 2017: Kvartsmineralogins betydelse för en lyckad luminiscensdatering. (15 hp)
515. Aldenius, Erik, 2017: Lunds Geotermisystem, en utvärdering av 30 års drift. (15 hp)
516. Aulin, Linda, 2017: Constraining the duration of eruptions of the Rangitoto volcano, New Zealand, using paleomagnetism. (15 hp)
517. Hydén, Christina Engberg, 2017: Drumlinerna i Löberöd - Spår efter flera isrörelseriktningar i mellersta Skåne. (15 hp)
518. Svantesson, Fredrik, 2017: Metodik för kartläggning och klassificering av erosion och släntstabilitet i vattendrag. (45 hp)
519. Stjern, Rebecka, 2017: Hur påverkas luminiscenssignaler från kvarts under laboratorieförhållanden? (15 hp)
520. Karlstedt, Filippa, 2017: P-T estimation of the metamorphism of gabbro to garnet amphibolite at Herrestad, Eastern Segment of the Sveconorwegian orogen. (45 hp)
521. Önnervik, Oscar, 2017: Ooider som naturliga arkiv för förändringar i havens geokemi och jordens klimat. (15 hp)
522. Nilsson, Hanna, 2017: Kartläggning av sand och naturgrus med hjälp av resistivitetsmätning på Själland, Danmark. (15 hp)
523. Christensson, Lisa, 2017: Geofysisk undersökning av grundvattenskydd för planerad reservvattentäkt i Mjölkalånga, Hässleholms kommun. (15 hp)
524. Stamsnijder, Joaen, 2017: New geochronological constraints on the Klipriviersberg Group: defining a new Neoarchean large igneous province on the Kaapvaal Craton, South Africa. (45 hp)
525. Becker Jensen, Amanda, 2017: Den eocena Furformationen i Danmark: exceptionella bevaringstillstånd har bidragit till att djurs mjukdelar fossiliserats.(15 hp)
526. Radomski, Jan, 2018: Carbonate sedimentology and carbon isotope stratigraphy of the Tallbacken-1 core, early Wenlock Slite Group, Gotland, Sweden. (45 hp)
527. Pettersson, Johan, 2018: Ultrastructure and biomolecular composition of sea turtle epidermal remains from the Campanian (Upper Cretaceous) North Sulphur River of Texas. (45 hp)
528. Jansson, Robin, 2018: Multidisciplinary perspective on a natural attenuation zone in a PCE contaminated aquifer. (45 hp)
529. Larsson, Alfred, 2018: Rb-Sr sphalerite data and implications for the source and timing of Pb-Zn deposits at the Caledonian margin in Sweden. (45 hp)
530. Balija, Fisnik, 2018: Stratigraphy and pyrite geochemistry of the Lower–Upper Ordovician in the Lerhamn and Fågelsång -3 drill cores, Scania, Sweden. (45 hp)
531. Höglund, Nikolas, 2018: Groundwater chemistry evaluation and a GIS-based approach for determining groundwater potential in Mörbylånga, Sweden. (45 hp)

532. Haag, Vendela, 2018: Studie av mikrostrukturer i karbonatslagkäglor från nedslagsstrukturen Charlevoix, Kanada. (15 hp)
533. Hebrard, Benoit, 2018: Antropocen – vad, när och hur? (15 hp)
534. Jancsak, Nathalie, 2018: Åtgärder mot kusterosion i Skåne, samt en fallstudie av erosionsskydden i Löderup, Ystad kommun. (15 hp)
535. Zachén, Gabriel, 2018: Mesosideriter – redogörelse av bildningsprocesser samt SEM-analys av Vaca Muertameteoriten. (15 hp)
536. Fägersten, Andreas, 2018: Lateral variability in the quantification of calcareous nannofossils in the Upper Triassic, Austria. (15 hp)
537. Hjertman, Anna, 2018: Förutsättningar för djupinfiltration av ytvatten från Ivösjön till Kristianstadbassängen. (15 hp)
538. Lagerstam, Clarence, 2018: Varför svalde svanödlor (Reptilia, Plesiosauria) stenar? (15 hp)
539. Pilser, Hannes, 2018: Mg/Ca i bottenlevande foraminiferer, särskilt med avseende på temperaturer nära 0°C. (15 hp)
540. Christiansen, Emma, 2018: Mikroplast på och i havsbotten - Utbredningen av mikroplaster i marina bottensediment och dess påverkan på marina miljöer. (15 hp)
541. Staahlnacke, Simon, 2018: En sammanställning av norra Skånes prekambriska berggrund. (15 hp)
542. Martell, Josefin, 2018: Shock metamorphic features in zircon grains from the Mien impact structure - clues to conditions during impact. (45 hp)
543. Chitindingu, Tawonga, 2018: Petrological characterization of the Cambrian sandstone reservoirs in the Baltic Basin, Sweden. (45 hp)
544. Chonewicz, Julia, 2018: Dimensionerande vattenförbrukning av grundvatten samt alternativa vattenkvaliteter. (15 hp)
545. Adeen, Lina, 2018: Hur lämpliga är de geofysiska metoderna resistivitet och IP för kartläggning av PFOS? (15 hp)
546. Nilsson Brunlid, Anette, 2018: Impact of southern Baltic sea-level changes on landscape development in the Verkeån River valley at Haväng, southern Sweden, during the early and mid Holocene. (45 hp)
547. Perälä, Jesper, 2018: Dynamic Recrystallization in the Sveconorwegian Frontal Wedge, Småland, southern Sweden. (45 hp)
548. Artursson, Christopher, 2018: Stratigraphy, sedimentology and geophysical assessment of the early Silurian Halla and Klinteberg formations, Altajme core, Gotland, Sweden. (45 hp)
549. Kempengren, Henrik, 2018: Att välja den mest hållbara efterbehandlingsmetoden vid sanering: Applicering av beslutsstödsverktyget SAMLA. (45 hp)
550. Andreasson, Dagnija, 2018: Assessment of using liquidity index for the approximation of undrained shear strength of clay tills in Scania. (45 hp)
551. Ahrenstedt, Viktor, 2018: The Neoproterozoic Visingsö Group of southern Sweden: Lithology, sequence stratigraphy and provenance of the Middle Formation. (45 hp)
552. Berglund, Marie, 2018: Basaltkuppen - ett spel om mineralogi och petrologi. (15 hp)
553. Hernnäs, Tove, 2018: Garnet amphibolite in the internal Eastern Segment, Sveconorwegian Province: monitors of metamorphic recrystallization at high temperature and pressure during Sveconorwegian orogeny. (45 hp)
554. Halling, Jenny, 2019: Characterization of black rust in reinforced concrete structures: analyses of field samples from southern Sweden. (45 hp)
555. Stevic, Marijana, 2019: Stratigraphy and dating of a lake sediment record from Lyngsjön, eastern Scania - human impact and aeolian sand deposition during the last millennium. (45 hp)
556. Rabanser, Monika, 2019: Processes of Lateral Moraine Formation at a Debris-covered Glacier, Suldenferner (Vedretta di Solda), Italy. (45 hp)

LUNDS UNIVERSITET